The Journal of Experimental Biology 207, 3813-3838
Published by The Company of Biologists 2004
doi:10.1242/jeb.01229

Neuromuscular control of aerodynamic forces and moments in the blowfly, *Calliphora vicina*

Claire N. Balint[1,*] and Michael H. Dickinson[2]

[1]*Department of Integrative Biology, University of California, Berkeley, CA 94720, USA* and [2]*Department of Bioengineering, California Institute of Technology, Pasadena, CA 91125, USA*

*Author for correspondence at present address: ARL Division of Neurobiology, PO Box 210077, University of Arizona, Tucson, AZ 85721, USA (e-mail: cnbalint@cal.berkeley.edu)

Accepted 4 August 2004

Summary

Flies are among the most agile of flying insects, a capacity that ultimately results from their nervous system's control over steering muscles and aerodynamic forces during flight. In order to investigate the relationships among neuromuscular control, musculoskeletal mechanics and flight forces, we captured high-speed, three-dimensional wing kinematics of the blowfly, *Calliphora vicina*, while simultaneously recording electromyogram signals from prominent steering muscles during visually induced turns. We used the quantified kinematics to calculate the translational and rotational components of aerodynamic forces and moments using a theoretical quasi-steady model of force generation, confirmed using a dynamically scaled mechanical model of a *Calliphora* wing. We identified three independently controlled features of the wingbeat trajectory – downstroke deviation, dorsal amplitude and mode. Modulation of each of these kinematic features corresponded to both activity in a distinct steering muscle group and a distinct manipulation of the aerodynamic force vector. This functional specificity resulted from the independent control of downstroke and upstroke forces rather than the independent control of separate aerodynamic mechanisms. The predicted contributions of each kinematic feature to body lift, thrust, roll, yaw and pitch are discussed.

Key words: insect flight, kinematics, aerodynamics, steering, motor control, *Calliphora vicina*.

Introduction

The basis for much of an insect's flight abilities lies in the deceptively simple back-and-forth flapping motion of its wings. The broad range of flight maneuvers displayed by flies, from subtle course corrections to sudden darts and saccades, suggests that wing motion can vary in complex ways. One of the challenges in understanding the flight motor system is to identify the components of wing motion that the fly can independently manipulate to produce an array of behavioral outputs.

Previously, studies have correlated specific features of wing kinematics to variation in aspects of free flight behavior such as forward velocity (Dudley and Ellington, 1990a; Ennos, 1989; Willmott and Ellington, 1997a). Other studies using tethered preparations have examined the kinematic correlates of lift and thrust control (Nachtigall and Roth, 1983; Vogel, 1967; Wortmann and Zarnack, 1993) and responses to sensory manipulations such as visual or mechanical roll and yaw (Faust, 1952; Hengstenberg et al., 1986; Lehmann and Dickinson, 1997; Srinivasan, 1977; Waldman and Zarnack, 1988; Zanker, 1990; Zarnack, 1988). However, the functional relationship between variation in wing motion and behavioral output has remained obscure due to two main complications. First, time-resolved, three-dimensional measurements of wing kinematics are difficult to acquire, especially over the duration of complete flight maneuvers. This difficulty forces a trade-off between the number of kinematic parameters that may be sensibly measured and the length of time over which they can be monitored. Although, 50 years ago, Weis-Fogh and Jensen (1956) emphasized the importance of simultaneous measurements of wing speed and angle of attack in particular for assessing the control of aerodynamic forces, such simultaneous measurements have been rare. Second, even detailed analyses of conventional kinematic parameters have been insufficient for predicting the resultant forces due to the significant influence of unsteady mechanisms (Cloupeau et al., 1979; Wilkin and Williams, 1993; Zanker and Gotz, 1990). Fortunately, recent advances in high-speed video technology have greatly facilitated the acquisition of detailed kinematic information (Fry et al., 2003). Due to an improved understanding of the contributions of delayed stall and rotational forces to quasi-steady approximations (Sane and Dickinson, 2001, 2002), detailed kinematic information, once obtained, can now be related to a reasonable approximation of the resultant aerodynamic forces. This improved understanding

of aerodynamic mechanisms has both confirmed the importance of gross kinematic features of wing motion (e.g. stroke amplitude, frequency) and emphasized the need for measurement and analysis of finer-scale kinematic variation.

In the present study, we used high-speed videography to quantify the changes in three-dimensional wing orientation with sufficient temporal resolution to estimate the resultant force vector at various stages of the wingbeat cycle and to confirm our estimate of force using a mechanical model. However, in contrast to most previous studies that categorized wingbeat kinematics (for review, see Taylor, 2001), as well as muscle activity (Kutsch et al., 2003; Spüler and Heide, 1978; Thüring, 1986; Waldman and Zarnack, 1988), according to the amount of force or torque produced, we organized our analysis based on particular features of wing motion we previously correlated with patterns of steering muscle activity. These features were 'downstroke deviation', a correlate of basalare muscle activity, and 'mode', a correlate of activity in the pteralae III and pteralae I muscles (Balint and Dickinson, 2001). Using a bottom-up approach building upon these previous findings and incorporating improved resolution of wing kinematics, we were able to bridge three levels of analysis: the correlation between steering muscle activity and wing kinematics, the mechanisms by which wing kinematics modify aerodynamic forces, and the contribution of aerodynamic forces to body forces and moments. The results of this approach suggest that it is the ability to manipulate the coupling among aerodynamically relevant kinematic parameters, rather than the ability to control these parameters independently, that allows *Calliphora vicina* the flexibility of control observed in previous measurements of its directional force and moment output (Blondeau, 1981; Schilstra and van Hateren, 1999).

Materials and methods

Tethering and filming procedure

Adult male blowflies, *Calliphora vicina* (R.-D.), were tethered and implanted with extracellular electrodes as described previously (Balint and Dickinson, 2001). Male flies were selected from a laboratory colony, maintained at approximately 22°C with a 12 h:12 h light:dark cycle. The age of all individuals was between one and two weeks post-eclosion at the time of tethering. Each tether was composed of a modified #0 insect pin soldered onto a 1.5 mm-diameter brass rod. Short lengths of 25 μm-diameter nickel chromium (NiChr) wire with formvar insulation (A-M Systems, Sequim, WA, USA) were soldered to the terminals of five pairs of 28-gauge wires, which were glued to the brass rod. Each fly was anesthetized by placing it in a –4°C freezer for 3–4 min, then immediately attached to the end of the insect pin with a mixture of collophonium and beeswax. We implanted the tips of a pair of the NiChr wires into each of five steering muscles (b2, b1, III1, I1, III2-4; nomenclature from Heide, 1968) on the left side of the animal. Flies were allowed to recover for one day following electrode implantation, and data were collected for 2–4 consecutive days following initial electrode implantation.

We secured the free end of the tether onto a piezoelectric crystal attached to a rigid acrylic rod. The acrylic rod was then secured onto a metal armature, so that the fly was held with its longitudinal body axis approximately 15° relative to the ground. The mouth of a small open-throat wind tunnel was positioned in front of the fly, ~5 cm from the front of the head. A 7.0×0.8 cm black cylindrical brass rod pendulum was suspended in front of the fly with the base of the rod level with the fly's head.

Three Kodak MotionPro cameras were positioned above, behind and on the left side of the fly (Fig. 1A). Each camera was positioned so that their lines of sight were orthogonal to each other and equidistant to the fly. We used identical 8.5 mm video lenses (Computar, Torrance, CA, USA) on each camera. Small panels of infrared light-emitting diodes (LEDs) placed opposite each camera acted as a backlight against which the fly was imaged. The wings were sufficiently translucent, such that the outline and venation were clearly visible in the camera image (Fig. 1B). We filmed the flies at a rate of 5000 frames s^{-1} and an electronic shutter speed of 1/20 000.

Extracellular potentials from the implanted electrodes were amplified using an AC amplifier (A-M Systems Model 1800) and digitized using a Digidata 1200 and Axoscope software (Axon Instruments, Union City, CA, USA). Oscillatory signals from the piezoelectric crystal, which were in phase with the stroke cycle, and frame-mark signals from the cameras were also recorded. All the signals were digitized at 37 kHz in order to adequately discriminate the 5000 Hz frame-mark signals. To initiate each flight bout, the wind tunnel was switched on and set to a wind speed of approximately 2 m s^{-1} at the mouth, and the pendulum rod was set into motion. When the fly reacted to the pendulum motion with stereotyped modulations of wing motions and steering muscle activity, we manually activated an external trigger to initiate video capture and electrophysiological data acquisition. Data were collected in this manner from seven animals.

Wing digitization

Captured images were directly downloaded to computer as bitmaps. The bitmap images were then analyzed using a custom digitizing program in MATLAB (Fry et al., 2003). For each time sample, the program displayed the synchronously captured images from each of the three cameras. Points were digitized simultaneously in all three fields. We digitized the *x*-, *y*- and *z*- coordinates of at least five points in each time sample: the anterior tip of the head, posterior tip of the abdomen, left wing hinge, left wingtip and right wing hinge. A sixth point, the right wingtip, was digitized when we chose to include information about the position of the right wing. Because the body was tethered and stationary, the head, tail and hinge coordinates were held constant for each sequence.

The coordinates of each point were transformed such that the wing hinge was the origin and the longitudinal body axis was tilted 50° relative to horizontal (Fig. 1C). The Cartesian

coordinates of the wingtip were then converted to spherical coordinates:

$$\theta = \tan^{-1}(y'/x'), \quad (1)$$

$$\phi = \tan^{-1}[z'/(x'^2 + y'^2)^{1/2}]. \quad (2)$$

A wire-frame image of a *Calliphora vicina* wing was then fit to match the hinge and tip coordinates and rotated about the hinge-to-tip axis until the wire-frame and wing outline matched best, as judged by eye. The digitized morphological wing angle, α, was the angle between the wire-frame plane and the vertical plane through the axis of rotation.

Using this procedure, we collected complete information about the wing position and orientation for each time point. Although bending and torsion of the wing were conspicuous during the upstroke and during wing rotations, these kinematic changes were excluded from our analysis. The left wing was digitized in a total of 19 523 time samples (569 wingbeat cycles), and the right wing was digitized in a total of 10 078 time samples (294 wingbeat cycles).

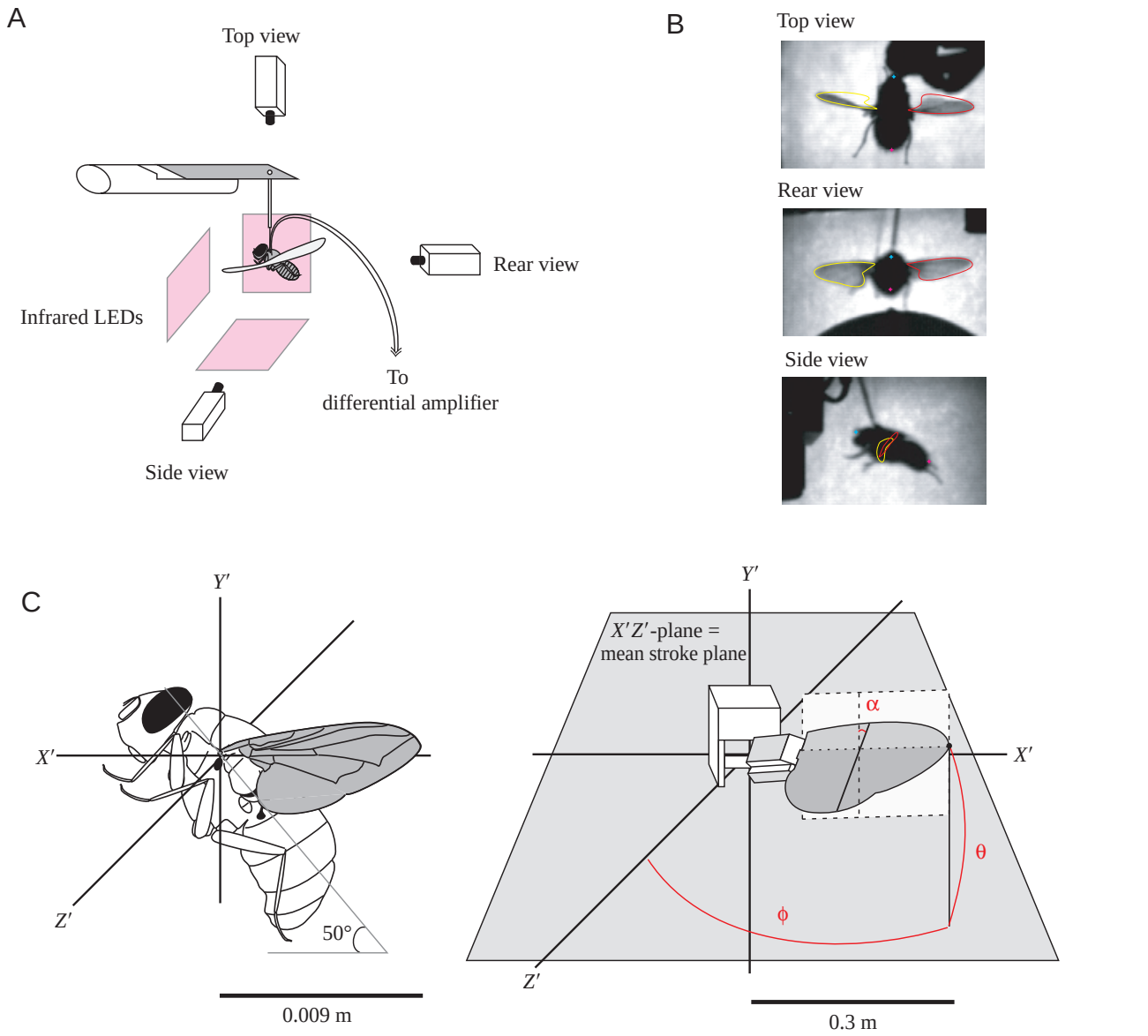

Fig. 1. Methods. (A) Schematic cartoon showing method of data collection (not drawn to scale). Tethered flies were positioned within view of three orthogonally arranged high-speed video cameras. A panel of infrared LEDs was placed opposite each camera to provide backlighting. (B) Sample video frame from each camera view. A wire frame image of a *Calliphora* wing (shown in yellow and red) was fit by eye to the outline of each wing in all three camera views simultaneously. The anterior tip of the head (blue cross) and the posterior tip of the abdomen (pink cross) were digitized once per sequence. (C) The wing's position at each time point was quantified relative to a 50°-tilted body axis (left). The progression of the three Euler angles (ϕ, θ and α) over time was reproduced using a mechanical model fitted with force transducers at the base of the model wing (right).

Force measurements

We used the mechanical model from previous studies (Fig. 1D; Dickinson et al., 1999; Sane and Dickinson, 2001, 2002) to measure the aerodynamic forces resulting from the measured wing kinematics. An enlarged planform of a *Calliphora vicina* wing was made by cutting a 2.3 mm-thick acrylic sheet into the shape of a wing isometrically scaled to 30 cm length and 7.6 cm mean chord length. The proximal end of the wing was attached to a two-dimensional force transducer and fixed to a gearbox driven in three rotational degrees of freedom by three servo-motors. The wing, force transducer and gearbox were immersed in mineral oil with a kinematic viscosity of 11.5 cSt.

A series of manipulations were performed on the wing data before replicating the kinematics on the dynamically scaled mechanical model. First, each sequence was divided into sets of 40 wingbeat cycles or fewer. Second, each of the three time series of wing angles (ϕ, θ, α) describing the first wingbeat cycle in each sequence was distorted so that the wing position at the beginning and end of the cycle was identical. This made it possible to repeat this cycle indefinitely without producing any sudden changes in position during transitions from one cycle to the next. This distorted version of the first wingbeat cycle was copied and concatenated into a series of four cycles and then added to the beginning of each data set. The last wingbeat cycle was similarly distorted, concatenated and added to the end of each data set. These sections of 'junk kinematics' allowed the mechanical model to reach speed and entrain the wake at the beginning of each sequence, and to slow down gradually at the end of the sequence, without affecting the kinematics of interest. Third, each of the three wing angle sequences was smoothed using a B-spline algorithm (based on criteria from Craven and Wahba, 1979) and temporally re-sampled so that motion between time points was 1° or less.

For each kinematic sequence, the mean wingbeat frequency of the mechanical model was scaled such that the Reynolds number (as defined by Ellington, 1984c) matched that of each fly. The mean wingbeat frequency observed among flight sequences ranged from 130 to 167 Hz. In order to match the Reynolds numbers for these sequences, the wingbeat frequencies reproduced by the mechanical model ranged from 0.125 to 0.145 Hz. Due to the large magnitude of the forces in this study and the effects of backlash in the gears linking the motors to the wing, the actual wing kinematics of the mechanical model differed depending on the direction of motion. To ameliorate these effects, we ran each sequence twice: once with the directional convention such that the wing moved from left to right for the downstroke and right to left for the upstroke ('forward'), and a second time such that the wing moved right to left for the downstroke and left to right for the upstroke ('backward'). We were able to minimize the directional bias due to backlash by using the 'backward' measurements for the downstroke and the 'forward' measurements for the upstroke.

The calibrated two-dimensional force transducer measured forces parallel and perpendicular to the wing. The voltage signals from the force transducer were acquired at a rate of 200 Hz using a data acquisition board (National Instruments, Austin, TX, USA) operated using a custom program written in MATLAB (see Sane and Dickinson, 2001, for more details). The gravitational contribution to the measured forces was subtracted, and the force signal was filtered offline using a low-pass digital Butterworth filter with a zero phase delay and a cut-off at 4 Hz. The resultant signal from the perpendicular channel was our measure of the total aerodynamic force normal to the wing (measured F_N). Because fly wings are relatively flat and flap at high angles of attack that separate flow, aerodynamic forces should be at all times roughly normal to the surface of the wing (Dickinson, 1996). Accordingly, we confirmed that the forces measured from the parallel channel were negligible.

The magnitude of forces measured using the mechanical model in oil are related to those of a fly flying in air by a simple conversion factor, as described previously (Fry et al., 2003):

$$F_{\text{fly}} = F_{\text{robot}} \frac{\rho_{\text{air}}\, \nu_{\text{fly}}\, \hat{r}_2^2\,(S)_{\text{fly}}}{\rho_{\text{oil}}\, \nu_{\text{robot}}\, \hat{r}_2^2\,(S)_{\text{robot}}} \ , \tag{3}$$

where F is the force magnitude, ρ is the fluid density, ν is the kinematic viscosity of the fluid, and $\hat{r}_2^2(S)$ is the non-dimensional second moment of wing area (Ellington, 1984a). We found the conversion factor in our experiments to be 0.0018. Therefore, all measured forces were multiplied by this factor in order to compare them with those expected for an actual fly.

Force calculations

Theoretical calculations of the quasi-steady translational and rotational components of aerodynamic force were made using the methods in Sane and Dickinson (2002). The translational force component normal to the wing surface was calculated as:

$$F_{\text{trans}} = \frac{\rho S U_t^2\, \hat{r}_2^2\,(S)}{2} [C_{\text{Lt}}^2\,(\alpha_g) + C_{\text{Dt}}^2\,(\alpha_g)]^{1/2} \ , \tag{4}$$

where S is the projected surface area of the wing, U_t is the wingtip velocity, and α_g is the wing's geometrical angle of attack with respect to its path. The lift (C_{Lt}) and drag coefficients (C_{Dt}) for the model wing were measured at a comparable Reynolds number and fitted with the following equations:

$$C_{\text{Lt}}(\alpha_g) = 0.015 + 1.98 \sin(1.92\alpha_g + 0.018) \tag{5}$$

and

$$C_{\text{Dt}}(\alpha_g) = 1.96 + 1.84 \cos(1.91\alpha_g + 3.15) \ . \tag{6}$$

The rotational force normal to the wing surface was calculated from:

$$F_{\text{rot}} = C_{\text{rot}} \rho U_t\, \omega \bar{c}^2 R \int_0^1 \hat{r}\hat{c}^2(\hat{r}) \mathrm{d}\hat{r} \ , \tag{7}$$

where ω is the absolute rotational angular velocity of the wing,

$\bar{c}$ is the mean chord length, R is the wing length, $\hat{r}$ is the non-dimensional radial position along the wing, and $\hat{c}(\hat{r})$ is the non-dimensional chord length (Ellington, 1984a). The rotational angular velocity, ω, is equivalent to the temporal derivative of α. Prior experiments have shown that the rotational force coefficient, C_{rot}, is dependent on the value of non-dimensional rotational angular velocity ($\hat{\omega}$; Sane and Dickinson, 2002):

$$\hat{\omega} = \omega \bar{c} U_t^{-1} . \quad (8)$$

To estimate rotational forces, we used the relationship between $\hat{\omega}$ and C_{rot} measured in Sane and Dickinson (2002) for model *Drosophila* wings. Although this must introduce some error in our estimates, these were deemed small relative to other sources of error based on inspection of the data. For instantaneous values of $\hat{\omega}$ of less than 0.123, C_{rot} was 0, and for values of $\hat{\omega}$ greater than or equal to 0.374, C_{rot} was 1.55. For values of $\hat{\omega}$ between 0.123 and 0.374:

$$C_{rot} = 6.175\hat{\omega} - 0.7596 . \quad (9)$$

Viscous forces that act parallel to the wing surface were ignored, a reasonable assumption at the Reynolds numbers used in this study.

The total aerodynamic force normal to the wing, F_N, was approximated as the sum of the translatory (F_{trans}) and rotational (F_{rot}) components normal to the wing. This model neglects two additional terms: added mass forces and wake capture forces, the latter resulting from the interaction between a wing and the shed vorticity of the previous strokes (Dickinson et al., 1999; Sane and Dickinson, 2002). However, using only translational and rotational components of the quasi-steady model, we obtained reasonably accurate approximations of the measured forces.

Rectangular components of force and moments relative to the body

The above measurements of the force normal to the wing surface were combined with the three-dimensional wing orientation relative to the body in order to calculate the directional components of force in the body's frame of reference. The wing angles were transformed such that the fly's longitudinal body axis was defined as the *X*-axis, its vertical axis was the *Y*-axis and its cross-sectional axis was the *Z*-axis (Fig. 2A). Note that this converted the reference frame from the inclined body axis used for assessing kinematic variation and reproducing the kinematics using the mechanical model (Fig. 1C,D) to a horizontal body axis (Fig. 2). The three-dimensional angular orientation of the wing directs the aerodynamic force into its rectangular components:

$$F_x = F_N \cos\alpha \cos\phi - F_N \sin\alpha \sin\theta \sin\phi , \quad (10)$$

$$F_y = F_N \sin\alpha \cos\theta , \quad (11)$$

$$F_z = -F_N \cos\alpha \sin\phi - F_N \sin\alpha \sin\theta \cos\phi , \quad (12)$$

where F_N is the total aerodynamic force normal to the wing, F_x is thrust, F_y is lift and F_z is the radial or sideslip force.

The contribution of the force vector to the body moment, **M**, is determined by:

$$\mathbf{M} = \mathbf{r} \times \mathbf{F_N} , \quad (13)$$

where **r** is the position vector between the body's center of mass and the wing's center of pressure, and $\mathbf{F_N}$ is the three-dimensional aerodynamic force vector normal to the wing surface. We estimated the center of mass as the point midway between the left and right wing hinge and used the wing's center of area (0.54*R* or 4.9 mm from wing base for a wing of 9 mm length) as an estimate of the wing's center of pressure. Roll (M_x), yaw (M_y) and pitch (M_z) moments were calculated from:

$$M_x = r_y F_z - r_z F_y , \quad (14)$$

$$M_y = r_z F_x - r_x F_z , \quad (15)$$

$$M_z = r_x F_y - r_y F_x . \quad (16)$$

Because the sideslip force (F_z) was small through our dataset,

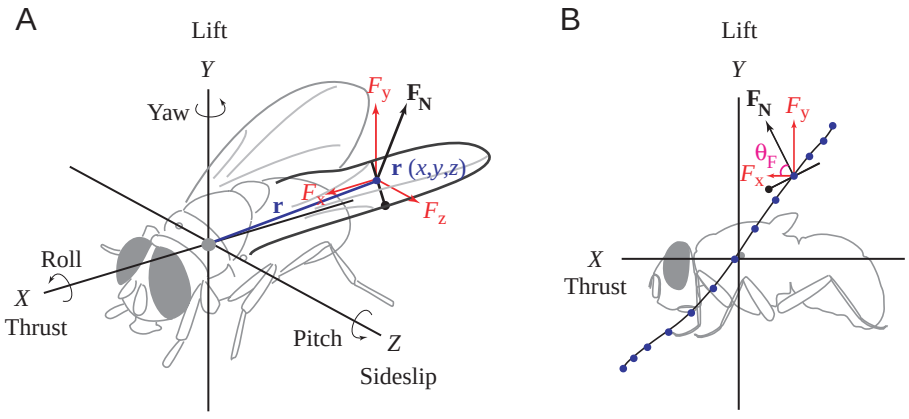

Fig. 2. Resultant forces and moments relative to the body. (A) Illustration of the six degrees of body motion: the directional components (thrust, lift and sideslip) and the moments (roll, yaw and pitch). The projection of the aerodynamic force vector ($\mathbf{F_N}$) onto each of the three rectangular axes constitutes its contribution to thrust (F_x), lift (F_y) and sideslip (F_z). The moment depends on the position vector **r** and the force vector $\mathbf{F_N}$ as described in the text. (B) Simplified sideview of A. If the sideslip component of force is negligible, lift and thrust depend primarily on the magnitude (F_N) and inclination (θ_F) of the force vector as the wing moves through the stroke (blue dots denote changes in position).

we were able to summarize the direction of the force vector as one angular measure, the force inclination (θ_F), thereby reducing the number of variables determining lift and thrust (Fig. 2B). The relationship between the force vector and the accompanying moment also simplifies, such that roll is essentially a function of lift (F_y), and yaw is essentially a function of thrust (F_x). Pitch remains a function of the difference between lift and thrust. Whereas roll and yaw are most sensitive to forces at mid-stroke when r_z is maximal (equations 14, 15), pitch is most greatly influenced by forces generated during stroke reversal when r_x and r_y are maximal (equation 16).

Results

Analytical framework

The goal of our analysis is to quantify the relationship between the kinematic adjustments correlated with steering muscle activity and the role of these adjustments in controlling aerodynamic forces during steering maneuvers. In order to study the relationship between muscle activity and body forces, we must bridge several intermediate levels of analysis that have been described previously. Therefore, the following discussion will introduce the known aspects of these intermediate transformations that were used for the combined analysis used in this study. First, we will describe the aspects of the aerodynamic force vector relevant to body forces and moments. Second, we will describe the kinematic variables relevant to control of aerodynamic forces. Third, we will describe the kinematic adjustments correlated with steering muscle activity. Finally, we will introduce the concerted nature of the changes accompanying each kinematic adjustment.

The motion of each wing contributes to the body's six degrees of freedom by varying the magnitude, direction and position of an aerodynamic force vector ($\mathbf{F_N}$; Fig. 2A). We found that in our study on *Calliphora*, the sideslip force generated by each wing was relatively small (maximum mean over wingbeat cycle: sideslip force 1.0×10^{-4} N *vs* lift and thrust forces 4.0×10^{-4} N). Therefore, the magnitude (F_N) and the inclination (θ_F) of the force vector were the primary output variables contributing to the remaining five degrees of freedom (Fig. 2B). Due to the dependence of moments on the instantaneous position of the wing, roll and yaw are most sensitive to forces at mid-stroke, whereas pitch is most sensitive to forces during stroke reversals.

The repetitive pattern of wing motion is characterized by a roughly harmonic back-and-forth motion, $\phi(t)$, during which the morphological wing angle is relatively constant until the wing rotates at the dorsal and ventral reversal points [$\alpha(t)$; Fig. 3A]. Variation in the wing deviation is relatively small throughout the wingbeat cycle and follows a more complicated waveform [$\theta(t)$; Fig. 3A]. According to a recent multi-component quasi-steady model (Sane and Dickinson, 2001, 2002), the primary kinematic determinants of aerodynamic force production are the wingtip velocity (U_t), the angle of attack (α_g) and the rotational angular velocity (ω; Fig. 3B). The tip velocity and the angle of attack together determine the translatory component of the force (F_{trans}), which reaches its peak during the middle of the stroke (Fig. 3C). The tip velocity and the rotational velocity together determine the rotational component of the force (F_{rot}), which acts from the end of one stroke to the beginning of the next (Fig. 3C). The sum of quasi-steady translatory and rotational force components is equal to the total calculated normal force. The time course of the calculated forces was in reasonably close agreement with forces measured by playing the kinematics on our dynamically scaled mechanical model (Fig. 3C). The main source of disagreement between the two traces was a positive transient in the measured forces at the start of each stroke that was not captured by the two-component quasi-steady model (Fig. 3C). This is the same pattern observed by Sane and Dickinson (2002) and is likely to be due to a combination of acceleration reaction (added mass) forces and wake capture.

Although a reasonably robust theory exists for predicting the forces resulting from an arbitrary change in wing motion, the link between aerodynamically relevant changes in wing kinematics and the activity of specific steering muscles is less clear. Our previous study (Balint and Dickinson, 2001) indicated that activity in specific steering muscles is well correlated with systematic and quantifiable distortions of the wingtip trajectory. In particular, displacement of the downstroke trajectory along the roughly anterio-posterior body axis, which we termed downstroke deviation, was a robust correlate of cycle-by-cycle activity patterns in the basalare muscles. However, changes in downstroke deviation were not isolated modulations of deviation, $\theta(t)$, but were consistently coupled with modulation of the ventral amplitude, the anterio-ventral maximum in elevation, $\phi(t)$. The ventral amplitude accompanying changes in downstroke deviation differed slightly depending on whether the muscles of pteralae III were active (Mode 2) or those of pteralae I were active (Mode 1). In the present study, our results concerning the correlation between muscle activity and these features of the wingtip trajectory were consistent with the previous findings (Fig. 4). However, our use of three-dimensional high-speed video in the present study allowed us to assess kinematic features related to changes in wing angle (α) in addition to changes in wingtip elevation (ϕ) and deviation (θ). We found that changes in wing angle [$\alpha(t)$] and wing trajectory [$\phi(t)$ and $\theta(t)$], rather than being independent of each other, were part of concerted kinematic programs. Therefore, downstroke deviation was one component of a three-dimensional kinematic alteration. In addition, the associated changes were not limited to the downstroke but extended over the entire cycle. The shape of the wingbeat trajectory, or the time course of $\theta(t)$ over the downstroke and following upstroke, was closely associated with downstroke deviation (Fig. 5A), as was the time course of the wing angle [$\alpha(t)$; Fig. 5B]. In addition, the ventral amplitude was correlated with downstroke deviation, except for the subtle de-coupling between modes (Fig. 5C), as mentioned above. The dorsal amplitude – the posterio-dorsal maximum in elevation – varied independently of downstroke

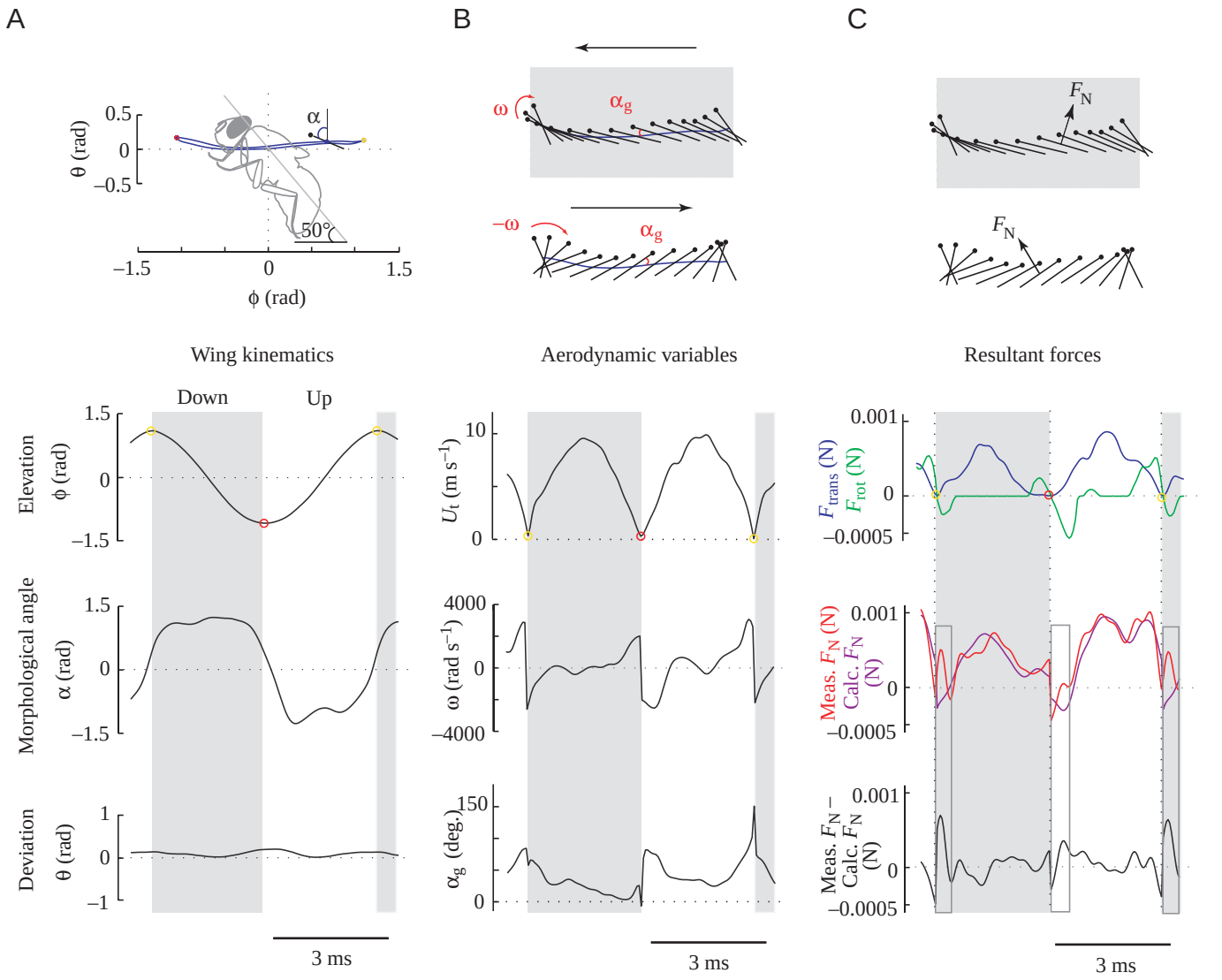

Fig. 3. Kinematic variables and aerodynamic forces over a wingbeat cycle. Yellow circles indicate the dorsal reversal, and the red circle indicates the ventral reversal point. (A) Representative time course of the three Euler angles describing wing orientation: elevation (ϕ), wing angle (α) and deviation (θ). (B) Accompanying time course of aerodynamically relevant variables: wingtip velocity (U_t), rotational velocity (ω) and angle of attack (α_g). (C) Resultant time course of forces: translatory (F_{trans}; blue) and rotational (F_{rot}; green) forces. The sum of translatory and rotational forces is equal to the calculated force (Calc. F_N; purple). The measured force (Meas. F_N; red) is the normal force measured using our dynamically scaled mechanical model. The wake capture force is the large discrepancy between measured and calculated force at the beginning of each half-stroke, indicated by the open gray boxes.

deviation and differed considerably between the two wings and across individuals (Fig. 5D). We also found that the wingbeat frequency was independent of downstroke deviation (Fig. 5E) and all other aspects of the wingbeat. The wingbeat frequency varied very little overall, and all individuals fell roughly into one of two frequency groups. However, the downstroke to upstroke ratio was correlated with downstroke deviation within trials (Fig. 5F) and was correlated with dorsal amplitude across trials (see Dorsal amplitude section below).

Given this combination of tightly and more loosely correlated features of wing motion, the functional significance of downstroke deviation as a control parameter is not directly evident in comparison with that of conventional uni-dimensional parameters such as total stroke amplitude, which theoretically correspond to a single aerodynamic variable, mean wingtip velocity (U_t). Within the entire data set, we identified three independently controlled features of the wingbeat trajectory: downstroke deviation, mode and dorsal amplitude. Downstroke deviation and mode were identified based on their robust match with patterns of muscle activity, whereas dorsal amplitude was identified based on its considerable inter-wing and inter-individual variability. For each of these components of the wingbeat trajectory, the associated changes were multi-dimensional and specific to different parts of the wingbeat cycle. We examined all changes in body forces and moments caused by alteration of these three

coordinated changes in wing motion. This approach consists of correlating the translatory forces (F_{trans}), rotational forces (F_{rot}) and force inclinations (θ_F) over each wingbeat cycle with each kinematic parameter and then summarizing the consequences for mean lift, thrust, roll, yaw and pitch. Through our analysis, we were able to confirm that these three kinematic patterns are distinct with respect to both behavioral function and neuromuscular control.

Downstroke deviation

As described in previous work (Balint and Dickinson, 2001), downstroke deviation was correlated on a cycle-by-cycle basis with the activity of the basalare muscles. However, the more thorough three-dimensional analysis showed that downstroke deviation accompanied a particular qualitative change in all three kinematic dimensions, $\phi(t)$, $\theta(t)$ and $\alpha(t)$, throughout each cycle. In order to quantify the functional significance of these coordinated changes for control of the aerodynamic force vector, we examined the influence of downstroke deviation on translational (F_{trans}) and rotational (F_{rot}) mechanisms of force generation, as well as the inclination of these forces (θ_F). This combination of influences will be used to demonstrate that the changes associated with downstroke deviation result in a predicted modulation of body lift *via* control of the force generated during the downstroke.

First, we investigated the changes relevant to control of the translatory force. As a consequence of the complex of kinematic parameters involved, changes in downstroke deviation were correlated with concerted changes of both angle of attack and tip velocity. More importantly, changes in downstroke deviation were not indicative of a mean change in these variables over the wingbeat cycle but rather a more complex change in time course throughout the stroke. Fig. 6A,D illustrates the pattern of variation in angle of attack that accompanied changes in downstroke deviation, and Fig. 6B,E illustrates the concomitant pattern of instantaneous tip velocity. Although both angle of attack and tip velocity varied throughout the cycle, the patterns of variation were quite distinct. During the downstroke, the angle of attack (Fig. 6A) and the tip velocity (Fig. 6B) varied in a complementary way, so that the dependence of the resultant force on downstroke deviation was relatively large (Fig. 6C). By contrast, during the upstroke, angle of attack (Fig. 6D) and tip velocity (Fig. 6E) varied inversely, such that the range of translatory force at each time point remained relatively small (Fig. 6F). Therefore, because of the precise pattern of changes in angle of attack and tip velocity, changes in downstroke deviation affected force during the downstroke but not the upstroke. In order to confirm the pattern of force modulation described above, we compared the relevant mid-stroke values for our experimental population.

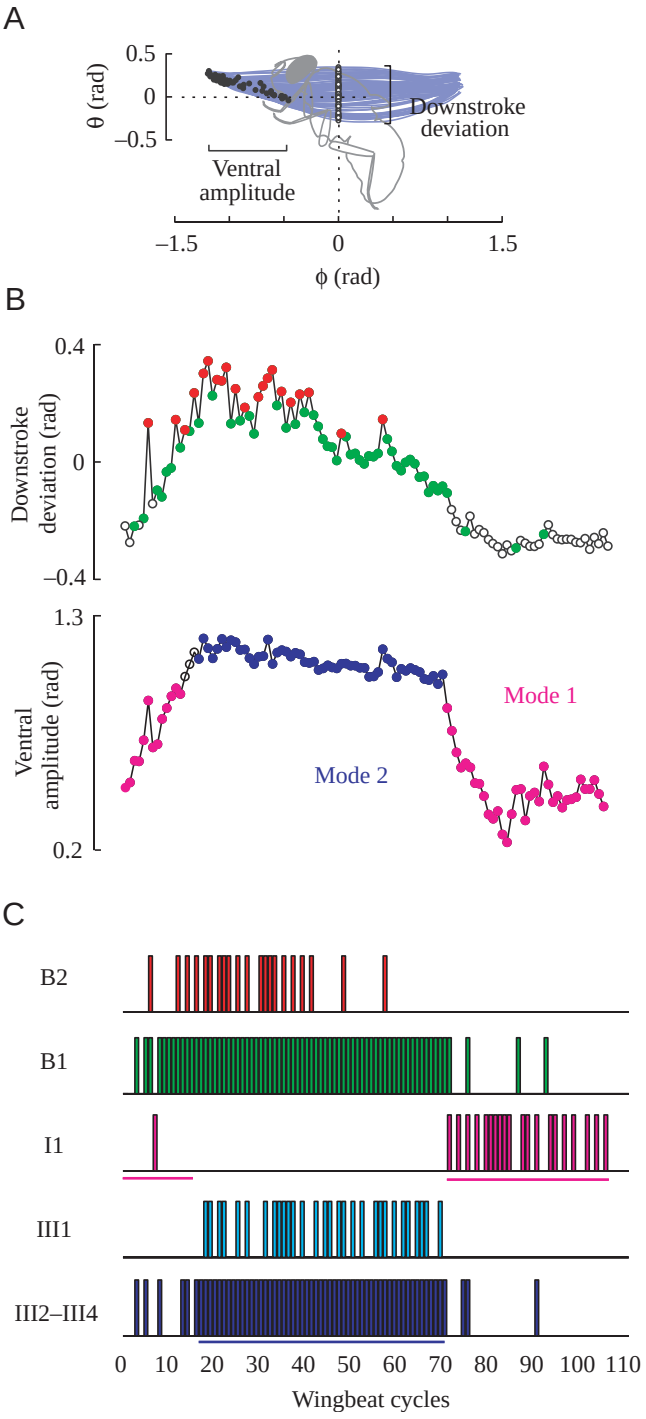

Fig. 4. Kinematic modulation in relation to muscle activity. (A) Characteristic range of downstroke tip trajectories. Downstroke deviation was defined as the deviation (θ) value at an elevation (ϕ) of 0 rad (indicated by white circles). Ventral amplitude was defined as the maximum elevation (ϕ) value during the ventral reversal (indicated by black circles). (B) Downstroke deviation and ventral amplitude of each cycle plotted as a function of time. Downstroke deviation points are color-coded according to the occurrence of a b2 and b1 spike (red), a b1 spike only (green) or the absence of basalare muscle spikes (open circles) within the cycle. Ventral amplitude points are color-coded according to burst activity in III2–4 (blue) or I1 (pink). The blue points were defined as Mode 2 and the pink points were defined as Mode 1. (C) Occurrence of spikes in muscles b2, b1, I1, III1 and III2–4. The blue, horizontal bar indicates maximal activity in III2–4, and the pink, horizontal bar indicates minimal activity in III2–4 paired with I1 activity. Plots in B and C share the same time scale.

For the downstroke, mid-stroke angle of attack, tip velocity and translatory force were consistently correlated with downstroke deviation (Fig. 7A), and the range of variation was similar to that shown in Fig. 6A–C. By contrast, angle of attack and tip velocity measured during the upstroke were much more variable across individuals (Fig. 7B). However, no inter-individual variation was evident in the upstroke translatory force (Fig. 7B). A subtle correlation existed between downstroke deviation and the upstroke translatory force, but upstroke force was consistently less variable than downstroke force.

Second, we investigated the associated changes in the rotational force. Although the mechanism for active control of rotation is not known (Ennos, 1988), we found a relatively strong correlation between downstroke deviation and the time course of the ventral rotation (Fig. 8A,B). By contrast, the timing and magnitude of the dorsal rotation was relatively constant. Whereas the ventral rotation elevates force at the end of the downstroke, it also acts to diminish total force at the start of the upstroke. As a consequence, ventral rotation contributed a small force to the end of the downstroke (Fig. 8C) that was complementary to the concomitant translatory force, so that

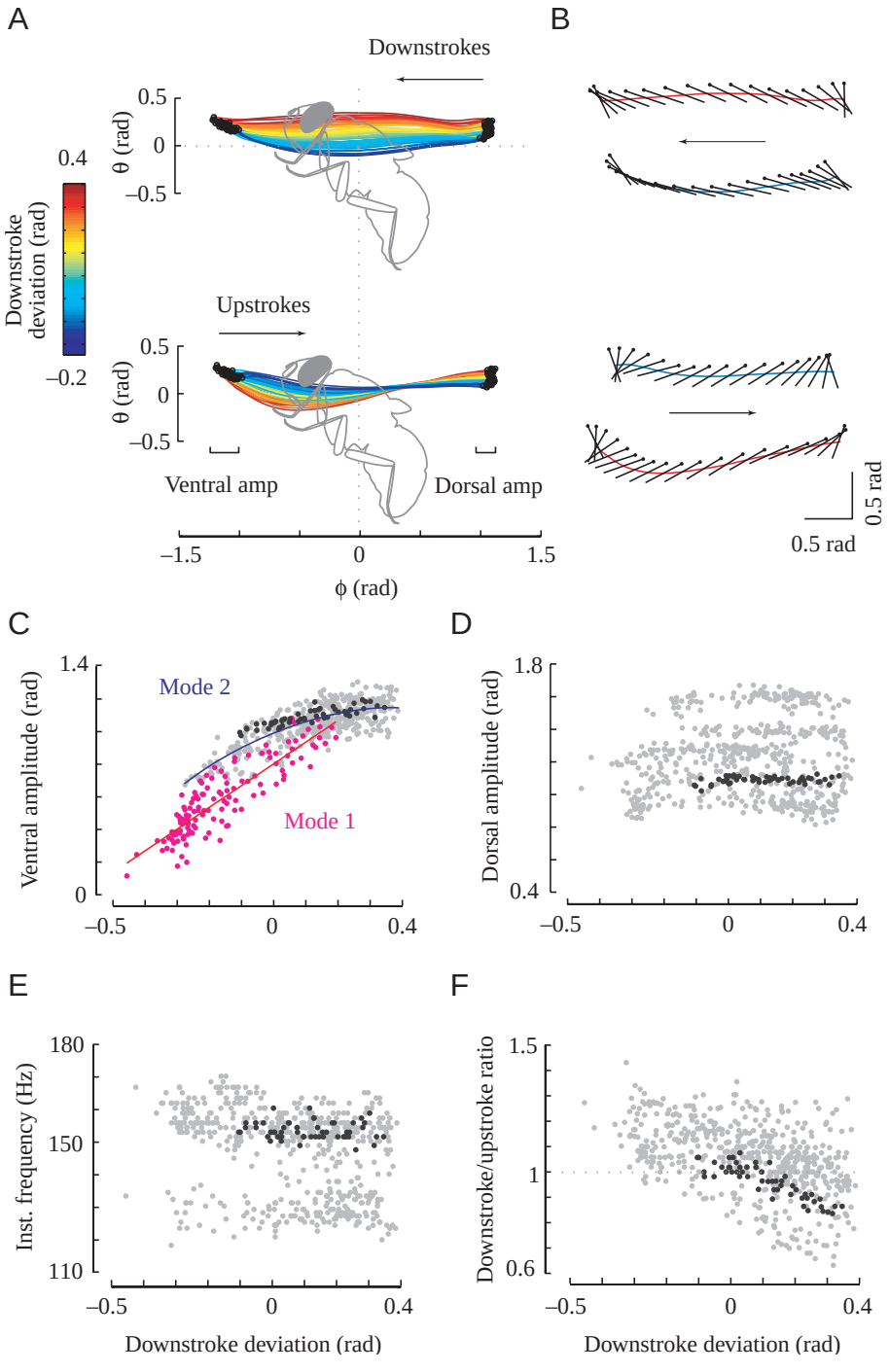

Fig. 5. Variation of kinematic parameters in relation to downstroke deviation. (A) Wingtip trajectories of downstrokes and accompanying upstrokes of a single individual, color-coded according to downstroke deviation value (color bar is shown on the left). Black circles indicate ventral and dorsal amplitudes. (B) Examples of wing orientations accompanying high (red) and low (blue) downstroke deviation, shown for the downstroke (above) and the upstroke (below). (C) Relationship between downstroke deviation and ventral amplitude within the experimental population (R^2=0.78). A subtle distinction exists between Mode 2 (gray points; blue line is a second order regression) and Mode 1 (pink points; red line). No distinction between modes was observed for the following parameters within the experimental population: relationship between downstroke deviation and (D) dorsal amplitude (R^2=0.02), (E) instantaneous wingbeat frequency (R^2=0.01) and (F) downstroke/upstroke ratio (R^2=0.30). Black circles in C–F indicate values for the individual shown in A.

both the rotational and translatory force components contributed to the correlation of downstroke deviation with total force (Fig. 8D). The ventral rotation contributed a large negative force to the start of the upstroke (Fig. 8F) due to the delay in wing rotation relative to stroke reversal (Fig. 8E), but addition of the concomitant positive translatory force resulted in a smaller range of total peak forces (Fig. 8G). The contribution of the dorsal rotational force to total force at the end of the upstroke was relatively large [mean rotational force peak, $5\times10^{-4}\pm1\times10^{-4}$ N (S.D.)], and its contribution to the

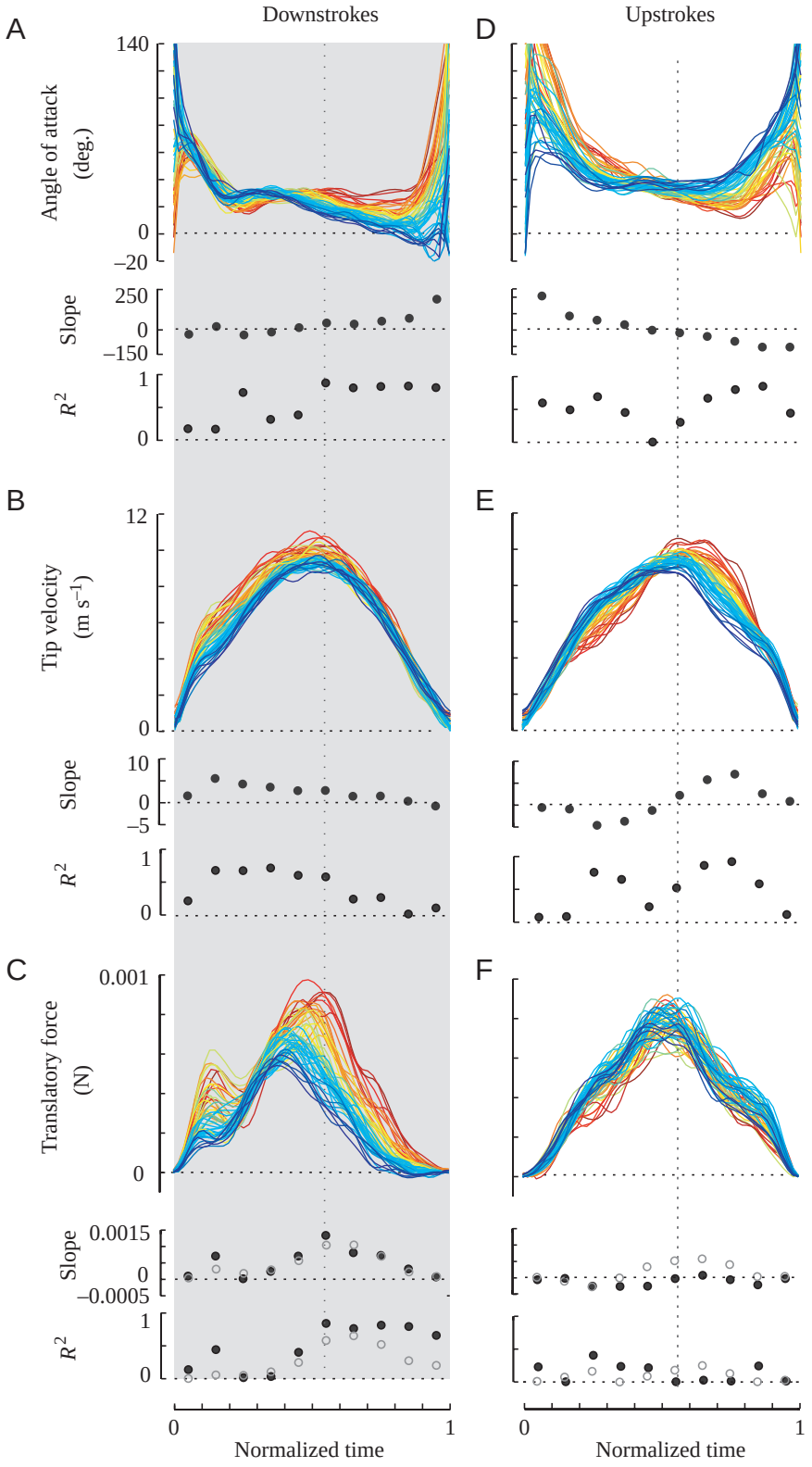

Fig. 6. Temporal variation in angle of attack, tip velocity and translatory force in a single individual, color-coded according to downstroke deviation as in Fig. 5A. All data are shown along a normalized time axis, where 0 is the beginning and 1 is the end of the half-stroke. The slope and R^2 regression statistics for the correlation between each parameter and downstroke deviation are shown for normalized time intervals of 0.05. Mid-stroke was defined as a normalized time of 0.55, indicated by the vertical dotted lines. (A) Angles of attack over the downstroke. (B) Tip velocities over the downstroke. (C) Translatory forces over the downstroke. Regression statistics are shown for the individual (black circles) and the population (gray circles). (D) Angles of attack over the upstroke. (E) Tip velocities over the upstroke. (F) Translatory forces over the upstroke. Regression statistics are shown for the individual (black circles) and the population (gray circles).

start of the downstroke was similar but more variable [mean rotational force peak, $-6\times10^{-4}\pm4\times10^{-4}$ N (S.D.)].

Third, we investigated the relationship between downstroke deviation and force inclination. The range and variability of force inclination differed between downstrokes and upstrokes, as did force magnitude. The force inclination over the downstroke was strongly correlated with downstroke deviation (Fig. 9Ai). Although the temporal pattern of force inclination was such that the sign of the correlation with downstroke deviation changes at mid-stroke, the overall variation was relatively small. The force was generally directed upward relative to the body, between roughly 60 and 80° relative to horizontal at the point of largest variation (Fig. 9Aii). By contrast, during the upstroke, force inclination was not correlated with downstroke deviation (Fig. 9Bi). The total aerodynamic force was generally directed forward relative to the body during the upstroke but varied over a wide range from –30 to 40° relative to horizontal across the experimental population (Fig. 9Bii). Therefore, downstrokes and upstrokes differed not only in the general direction of the force vector but also with respect to the degree of variation in force inclination.

Finally, we assessed the influence of downstroke deviation on mean resultant forces and moments. The overall dichotomy between downstrokes and upstrokes was that, during the downstroke, the force magnitude was variable (Fig. 10A,B) while the force inclination was relatively constant (Fig. 10A,C) whereas, during the upstroke, the force magnitude was relatively constant (Fig. 10F,G) while the force inclination was variable (Fig. 10F,H). The modulation of force magnitude during the downstroke resulted mainly in modulation of lift (Fig. 10D) and roll (Fig. 10E). The small changes in force magnitude during the upstroke resulted in a relatively constant thrust (Fig. 10I) and yaw (Fig. 10J). The uncorrelated variation in upstroke force inclination had a greater effect on lift and roll than on thrust (Fig. 10I,J). The asymmetry between the variable downstroke lift and the less variable upstroke thrust resulted in modulation of the mean pitch over each cycle that was well correlated with the downstroke deviation within individuals (Fig. 11A). However, the uncorrelated lift component during the upstrokes (Fig. 11B) resulted in inter-individual variation in pitch (Fig. 11A).

In conclusion, the primary role of changes in downstroke deviation and the associated kinematic variables by the

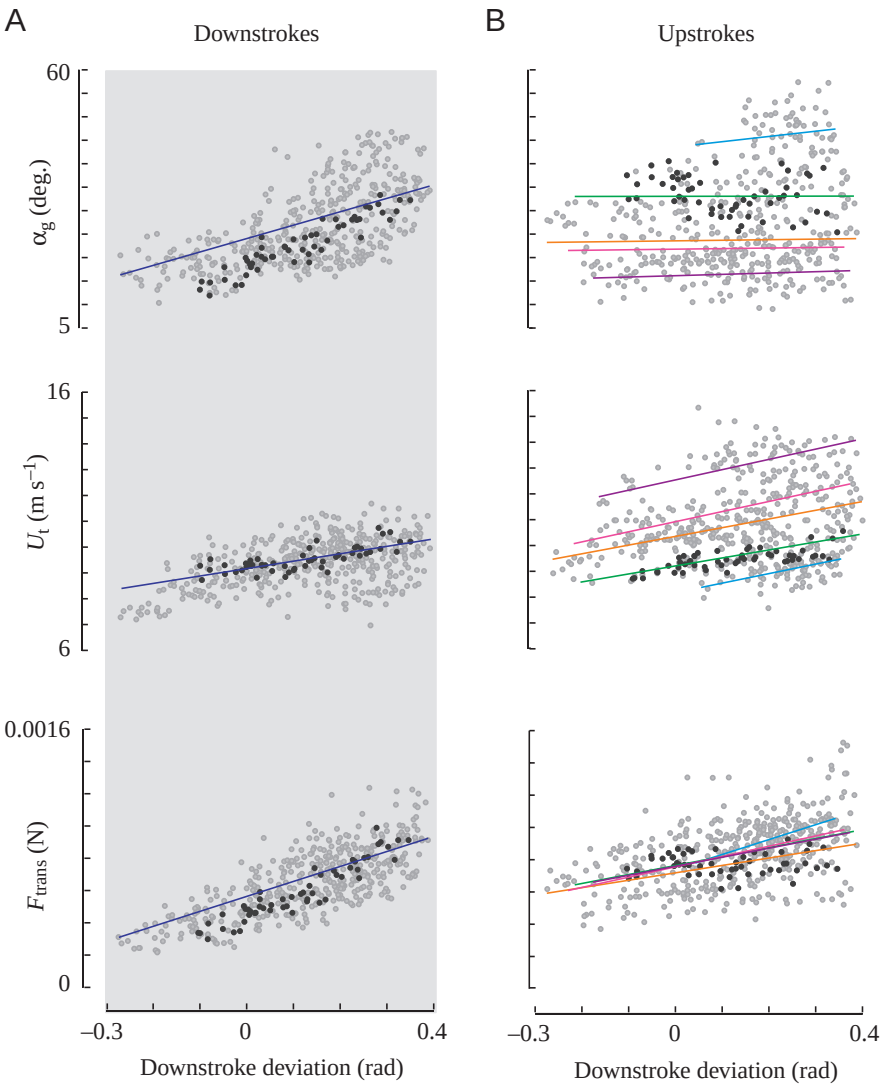

Fig. 7. Correlation between downstroke deviation and the mid-stroke angle of attack, tip velocity and translatory force for the experimental population. Black circles indicate values for the individual shown in Fig. 6. (A) Correlation between downstroke deviation and mid-downstroke angle of attack (R^2=0.41), tip velocity (R^2=0.22) and translatory force (R^2=0.58). (B) Correlation between downstroke deviation and mid-upstroke angle of attack (R^2=0.06), tip velocity (R^2=0.05) and translatory force (R^2=0.23). Five separate regressions are shown for five individuals.

basalare muscles was to modulate the lift force generated during the downstroke and thereby induce a roll moment as well as some pitch. The accompanying kinematic changes also produced a more subtle modulation of thrust and yaw during the upstroke.

Dorsal amplitude

Dorsal amplitude was a component of wing motion that remained relatively constant as downstroke deviation varied. Because variation of dorsal amplitude was small within individuals, we were unable to correlate differences with any

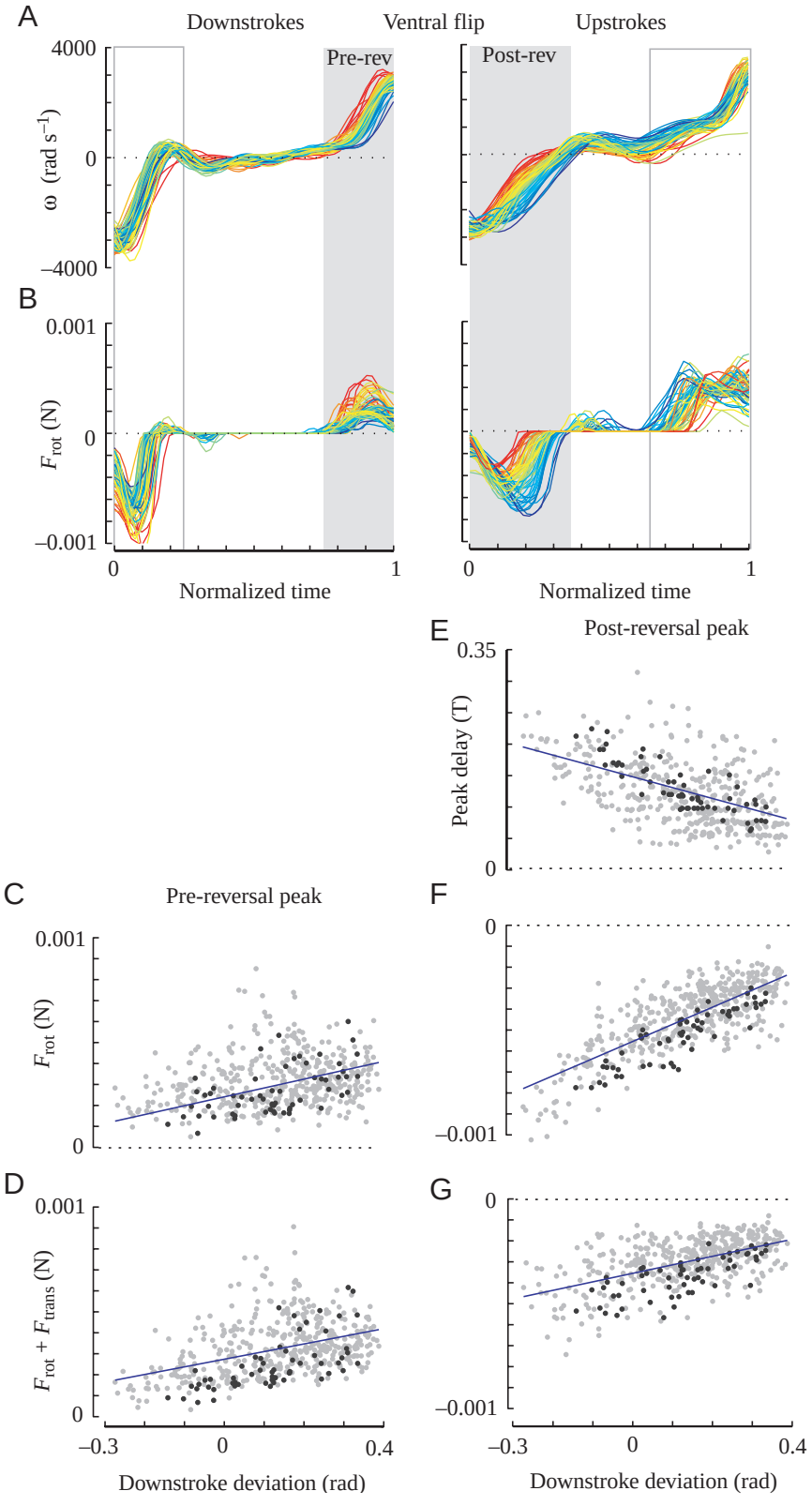

Fig. 8. Correlation between downstroke deviation and rotational forces. (A) Time course of rotational velocities and (B) time course of rotational forces for a single individual, color-coded according to downstroke deviation. Data are shown over a normalized time axis for the downstroke and upstroke. The filled gray box indicates the ventral rotation, and the open gray box indicates the dorsal rotation. For the ventral rotation, the pre-reversal portion occurs at the end of the downstroke, and the post-reversal portion occurs at the beginning of the upstroke. (C–G) The following data are for the experimental population. Black circles indicate values for the individual shown in A and B. Correlation between downstroke deviation and (C) pre-reversal peak rotational force (R^2=0.07), (D) pre-reversal total force peak (R^2=0.20), (E) post-reversal normalized time delay of rotational force peak (R^2=0.15), (F) post-reversal peak rotational force (R^2=0.60) and (G) post-reversal total force peak (R^2=0.31).

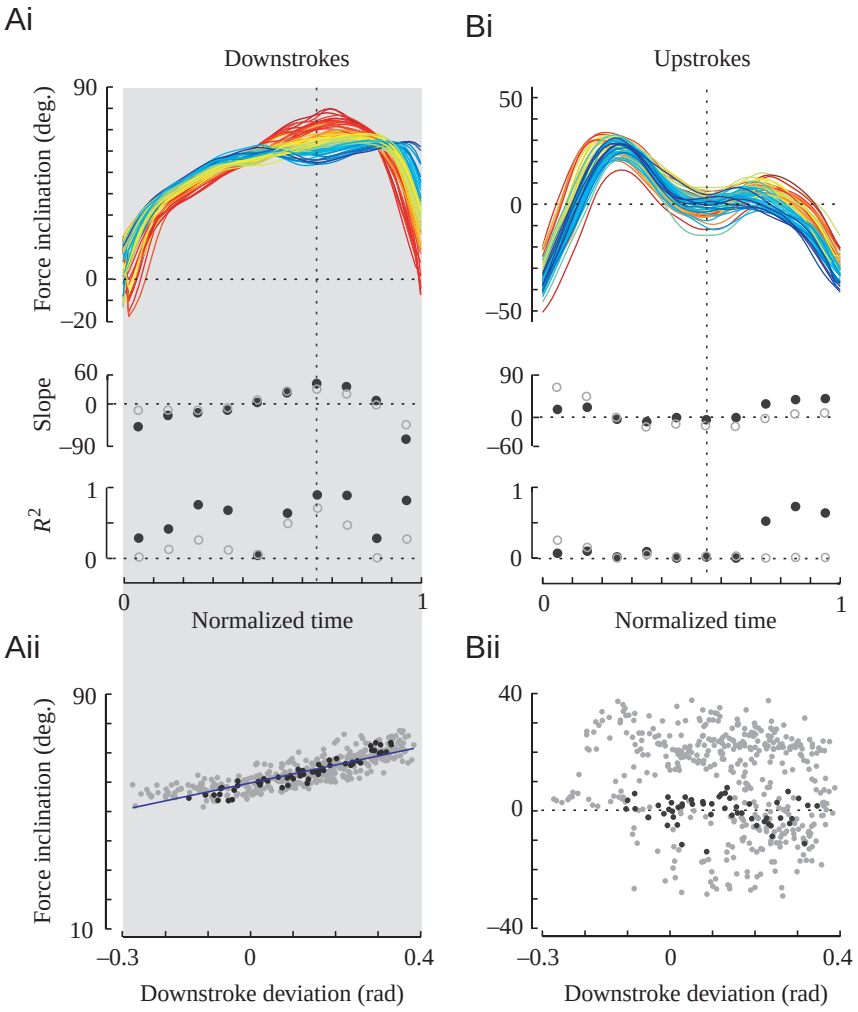

Fig. 9. Correlation between downstroke deviation and force inclination. (Ai) Time course of force inclination during the downstroke for a single individual, color-coded according to downstroke deviation. The slope and R^2 regression statistics for the correlation between downstroke deviation and force inclination are shown for normalized time intervals of 0.05. Regression statistics are shown for the individual (black circles) and the population (gray circles). The vertical dotted line indicates a normalized time of 0.65. (Aii) Correlation between downstroke deviation and the mid-downstroke (normalized time 0.65) force inclination for the experimental population (R^2=0.71). Black circles indicate data for the individual in Ai. (Bi) Time course of force inclination during the upstroke for a single individual, color-coded according to downstroke deviation. The slope and R^2 regression statistics for the correlation between downstroke deviation and force inclination are shown at the bottom, as in Ai. The vertical dotted line indicates a normalized time of 0.55. (Bii) Correlation between downstroke deviation and mid-upstroke (normalized time 0.55) force inclination for the experimental population (R^2=0.03). Black circles indicate data for the individual in Bi.

pattern of muscle activity. However, inter-wing and inter-individual variation in dorsal amplitude was considerable. Therefore, we investigated the relationship of dorsal amplitude to the inter-individual variation in the upstroke parameters that were unexplained with respect to downstroke deviation. We will demonstrate that the changes associated with dorsal amplitude result in a predictable modulation of body lift *via* inclination of the force vector during the upstroke.

Although dorsal amplitude was not associated with any significant differences in the shape of the wingtip trajectory [$\theta(t)$; Fig. 12A], it did accompany differences in morphological wing angle during the upstroke [$\alpha(t)$; Fig. 12B]. Inter-individual differences in the downstroke to upstroke ratio were also correlated with dorsal amplitude (Fig. 12C). As a consequence of the coupling of morphological wing angle and amplitude, changes in dorsal amplitude resulted in concerted changes of both the geometrical angle of attack and the tip velocity during the upstrokes. Fig. 13Ai illustrates the variation in the angle of attack through the upstroke for three sample individuals differing in dorsal amplitude. Among these three individuals, as well as across the experimental population, the mid-stroke angle of attack was negatively correlated with dorsal amplitude (Fig. 13Aii). Thus, the angle of attack was lower in upstrokes that extended to a more dorsal position. At the same time, the upstroke tip velocity of these individuals (Fig. 13Bi), as well as across all individuals (Fig. 13Bii), was positively correlated with dorsal amplitude. Therefore, due to the inverse relationship between angle of attack and tip velocity, translatory force showed little variation with respect to dorsal amplitude (Fig. 13C). We also found no relationship between dorsal amplitude and rotational force (data not shown).

The associated variation in morphological wing angle resulted in alteration of both the geometrical angle of attack and force inclination. Whereas dorsal amplitude was negatively correlated with upstroke angle of attack, it was positively correlated with force inclination. The correlation between dorsal amplitude and force inclination was strong from the middle to the end of the upstroke, across all individuals (Fig. 14A,B). In contrast to this variation in force inclination, the kinematic changes associated with dorsal amplitude resulted in a constant force magnitude (Fig. 15B,C). As a result, the mean lift varied with dorsal amplitude more strongly than mean thrust (Fig. 15D). As expected, the variation in roll followed the variation in lift (Fig. 15E).

Therefore, the inter-individual variation in upstroke lift and roll (Fig. 10I,J) and mean pitch (Fig. 11) that was uncorrelated with downstroke deviation may be explained by independent, inter-individual differences in dorsal amplitude (dorsal amplitude *vs* mean pitch, R^2=0.58).

In conclusion, the primary role of changes in dorsal amplitude and the associated kinematic variables was to enhance the lift during the upstroke by tilting the force vector and thereby contribute to variation in roll and pitch moments.

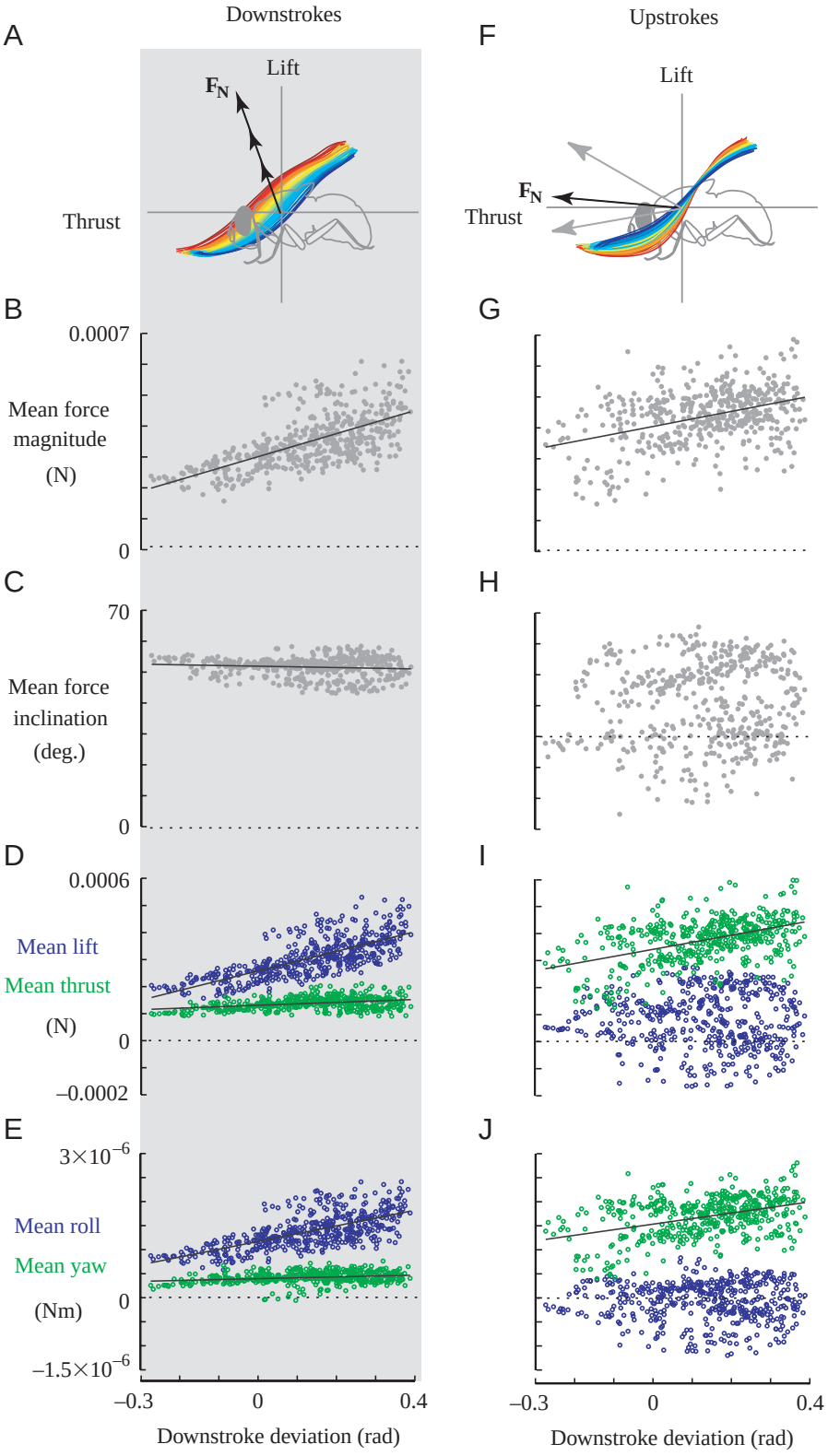

Fig. 10. Mean force vector ($\mathbf{F_N}$) and resultant directional forces and moments. (A) Schematic illustrating the type of force vector modulation occurring during the downstroke. As downstroke deviation changes, there is a correlated modulation of force magnitude while force inclination remains relatively constant. Correlation between downstroke deviation and downstroke (B) mean force magnitude (R^2=0.43), (C) mean force inclination (R^2=0.02), (D) mean lift (blue; R^2=0.54) and mean thrust (green; R^2=0.13), and (E) mean roll (blue; R^2=0.44) and mean yaw (green; R^2=0.05). (F) Schematic illustrating primary type of variation in mean force vector during the upstroke. As downstroke deviation changes, force magnitude is relatively constant, but there is unexplained variation in force inclination. Correlation between downstroke deviation and upstroke (G) mean force magnitude (R^2=0.16), (H) mean force inclination (R^2=0.004), (I) mean thrust (green; R^2=0.22) and mean lift (blue; R^2=0.0001), and (J) mean yaw (green; R^2=0.17) and mean roll (blue; R^2=0.001). The direction of the roll and yaw moments in E and J differ depending on whether they are generated by the left or right wing. For the left wing, positive roll is a right side down roll, and positive yaw is a yaw to the right. For the right wing, positive roll is a left side down roll, and positive yaw is a yaw to the left.

Mode

The most obvious characteristic of wingtip trajectories that correlated with changes in the activity of the muscles of pterale I and III was a shift in the ventral amplitude accompanying changes in downstroke deviation. We termed this qualitative alteration in stroke pattern a mode shift. Although no other noticeable changes in the downstroke trajectory were associated with differences in mode, the upstroke trajectory was slightly lower in deviation during Mode 1 than during Mode 2 (Fig. 16A). In addition, the upstroke wing angles differed between modes (Fig. 16B). Although we defined a change in mode as a roughly binary shift in ventral amplitude, we did observe graded, intra-mode variation in ventral amplitude accompanying changes in downstroke deviation, as well as inter-individual variation in dorsal amplitude. We examined the functional significance of mode shift by comparing the changes associated with downstroke deviation and dorsal amplitude within Mode 1 strokes, with changes associated with the same parameters within Mode 2 strokes. We will demonstrate that the kinematic changes specific to a mode shift result in a predicted modulation of body thrust due to a change in the force generated during the upstroke.

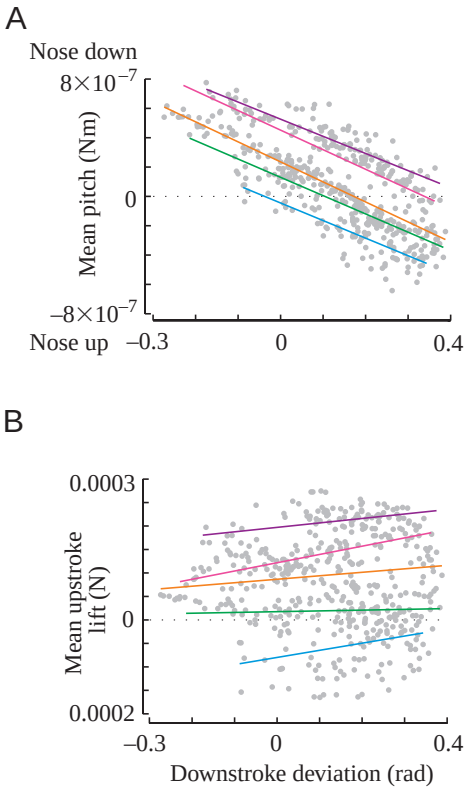

Fig. 11. Mean pitch. (A) Correlation between downstroke deviation and mean pitch from each wingbeat cycle. Regression lines for five individuals super-imposed. A relatively strong correlation exists within each individual (R^2=0.65 turquoise, 0.87 green, 0.97 orange, 0.83 pink, 0.76 purple), but the correlation differs across individuals (total R^2=0.49). (B) Upstroke lift from Fig. 10I, with regression lines for the same five individuals from A super-imposed.

Fig. 17 compares the temporal pattern of angle of attack, tip velocity and translatory force associated with Mode 1 and 2 strokes. An equivalent range of downstroke deviations is represented in each mode, and dorsal amplitude is constant. For the downstroke, the angle of attack tended to be greater during Mode 1, most dramatically at the beginning and end of the stroke (Fig. 17A). By contrast, tip velocities tended to be slightly lower during Mode 1 but overlapped with those of Mode 2 (Fig. 17B). The resultant range of translatory forces was equivalent within both modes, although the force onset was slightly delayed in Mode 1 strokes (Fig. 17C). For the upstroke, the angle of attack was generally lower during Mode 1 (Fig. 17D), whereas the tip velocities also tended to be lower during Mode 1 but overlapped with those during Mode 2 (Fig. 17E). However, because the changes in angle of attack and tip velocity were complementary, the translatory force during the upstroke was much greater in Mode 2 strokes than in Mode 1 strokes (Fig. 17F).

Comparing the mid-stroke values over our experimental

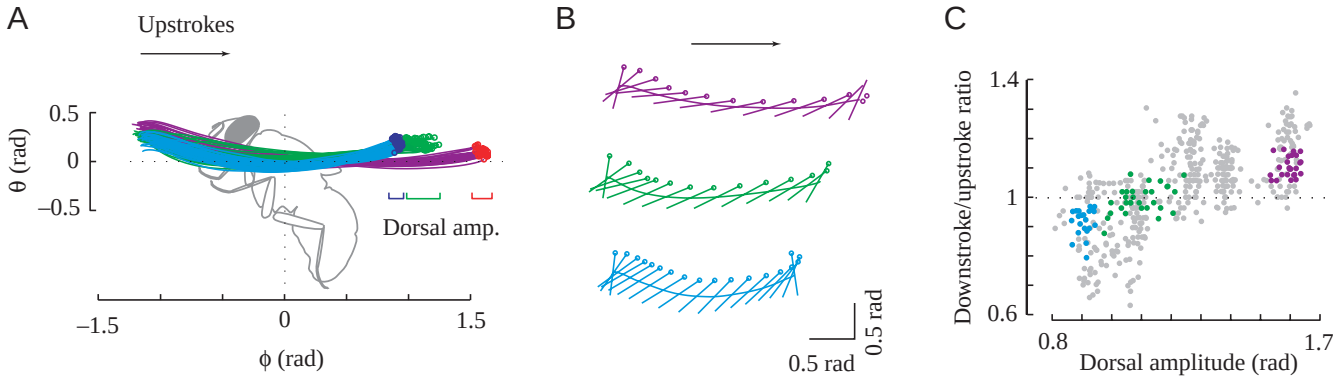

Fig. 12. Variation of kinematic parameters in relation to dorsal amplitude. (A) Wingtip trajectories during the upstroke, shown for three individuals differing in dorsal amplitude. Colored circles indicate dorsal amplitudes. (B) Examples of wing orientations accompanying large (purple), intermediate (green) and small (turquoise) dorsal amplitude during the upstroke. (C) Relationship between dorsal amplitude and downstroke/upstroke ratio within the experimental population (R^2=0.45). Colored circles indicate data for the three individuals shown in A.

population, we found that, for the downstroke, the relationship of angle of attack and tip velocity with downstroke deviation was similar within both modes, but with minor differences. Whereas the angle of attack during Mode 1 strokes was occasionally large, the accompanying tip velocity was comparatively small. Due to a consistent relationship between angle of attack and tip velocity, the correlation between downstroke deviation and translatory force remained nearly identical for both modes (Fig. 18A). For the upstroke, we compared the relationship of angle of attack and tip velocity

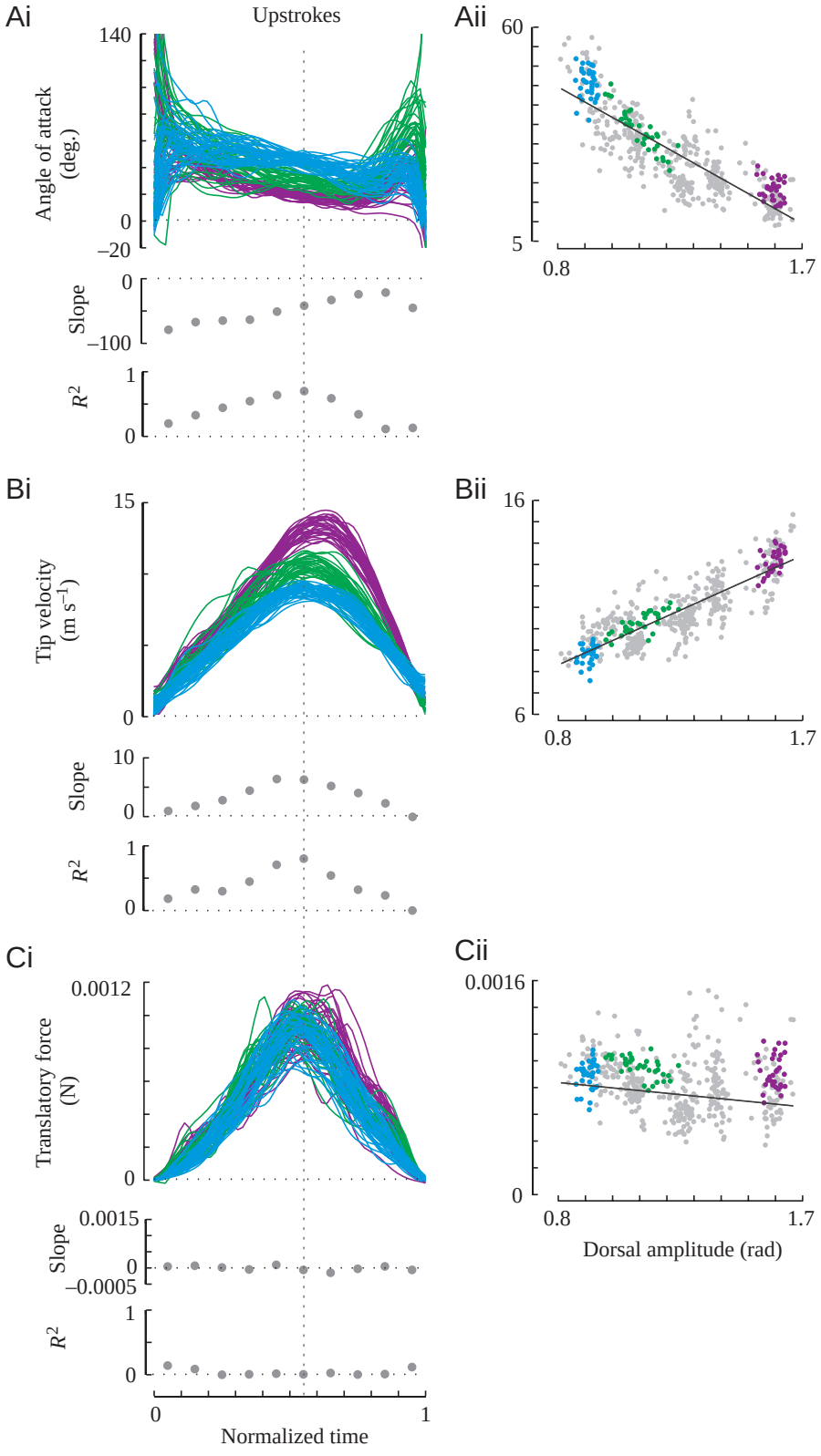

Fig. 13. Correlation between dorsal amplitude and upstroke translatory forces. Colors indicate data from three individuals with large (purple), intermediate (green) and small (turquoise) dorsal amplitudes. All time-course data are shown along a normalized time axis. The slope and R^2 regression statistics for the correlation between each parameter and dorsal amplitude are shown for normalized time intervals of 0.05. Mid-upstroke was defined as a normalized time of 0.55, indicated by the vertical dotted line. (Ai) Time course of the angle of attack over the upstroke, shown for three individuals. (Aii) Correlation between dorsal amplitude and mid-upstroke angle of attack, for the experimental population (R^2=0.71). (Bi) Time course of the tip velocity over the upstroke, shown for three individuals. (Bii) Correlation between dorsal amplitude and mid-upstroke tip velocity, for the experimental population (R^2=0.73). (Ci) Time course of the translatory force over the upstroke, shown for three individuals. (Cii) Correlation between dorsal amplitude and mid-upstroke translatory force, for the experimental population (R^2=0.04).

with dorsal amplitude between modes. The angle of attack was consistently lower during Mode 1 strokes than during Mode 2 strokes (Fig. 18B). The tip velocities were slightly lower during Mode 1 strokes but overlapped with those within Mode 2. However, due to the consistently lower angle of attack, the translatory force was consistently lower during Mode 1 than during Mode 2 strokes, even when the tip velocities overlapped (Fig. 18B). The mid-upstroke translatory forces were subtly correlated with downstroke deviation within both modes (Fig. 18C).

Fig. 19A,B compares the time course of rotation and rotational force during Mode 1 with that during Mode 2. Mode 1 was associated with a delay in the rotational peak at the

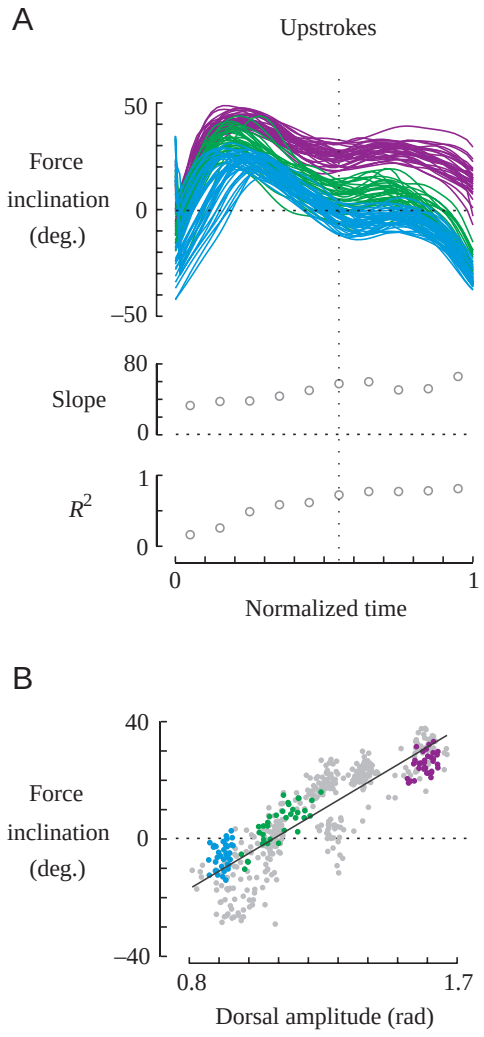

Fig. 14. Correlation between dorsal amplitude and upstroke force inclination. (A) Time course of force inclination during the upstroke, shown for the three individuals in Fig. 13. The slope and R^2 regression statistics for the correlation between dorsal amplitude and force inclination in normalized time intervals of 0.05 for the experimental population are shown at the bottom. Mid-upstroke, defined as a normalized time of 0.55, is indicated by the vertical dotted line. (B) Correlation between dorsal amplitude and mid-upstroke force inclination for the experimental population (R^2=0.76).

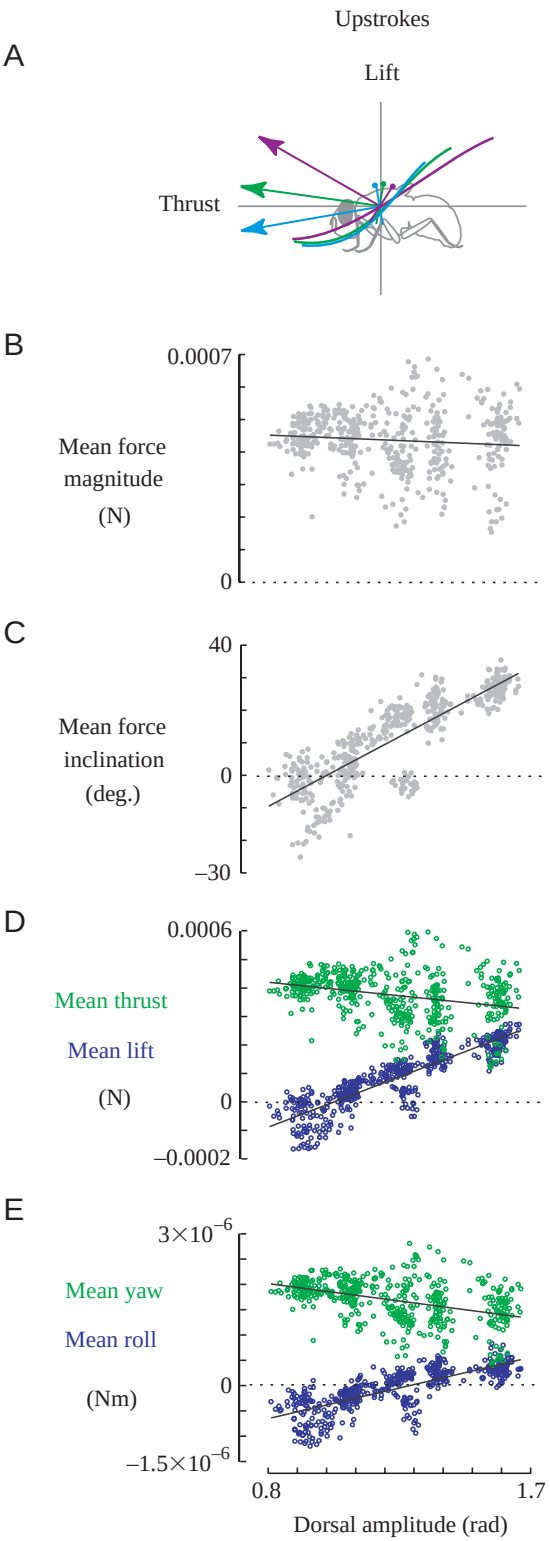

Fig. 15. Mean force vector and resultant directional forces and moments. (A) Schematic illustrating primary type of variation in mean force vector during the upstroke as in Fig. 10F. Differences in force inclination were well correlated with dorsal amplitude. Correlation between dorsal amplitude and upstroke (B) mean force magnitude (R^2=0.009), (C) mean force inclination (R^2=0.75), (D) mean lift (blue; R^2=0.79) and mean thrust (green; R^2=0.09), and (E) mean roll (blue; R^2=0.58) and mean yaw (green; R^2=0.18).

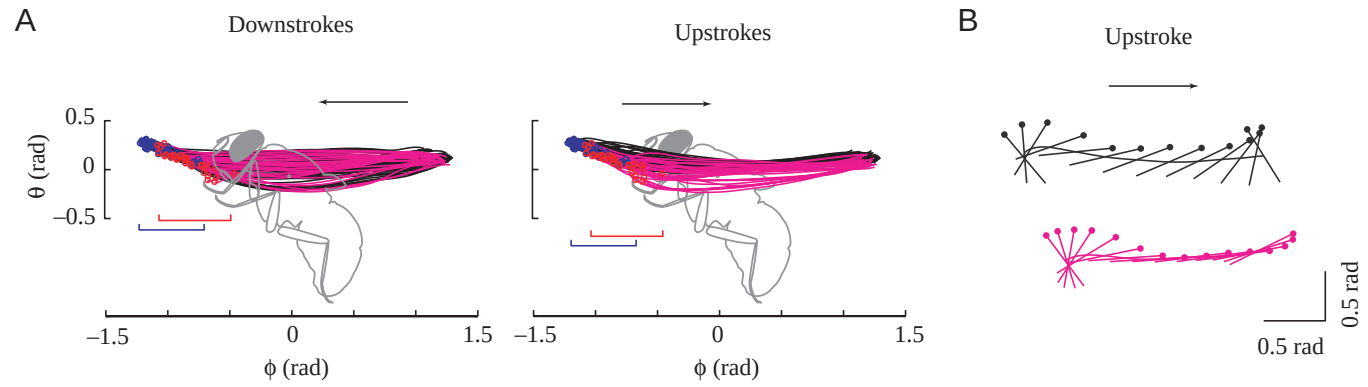

Fig. 16. Variation of kinematic parameters in relation to mode. (A) Comparison of wingtip trajectories during Mode 2 (black) and Mode 1 (pink). Blue circles indicate ventral amplitudes during Mode 2, and red circles indicate ventral amplitudes during Mode 1. (B) Examples of wing orientations during the upstroke for Mode 2 (black) and Mode 1 (pink).

beginning of the downstroke (Fig. 19C). This means that the dorsal flip was substantially delayed during Mode 1 strokes. Although this delay was not correlated with a consistent change in the magnitude of the rotational force peak at the beginning of the downstroke (Fig. 19D), it was correlated with a decrease in the magnitude of the rotational force peak at the end of the upstroke (Fig. 19F). Although the difference in rotational force at the end of the upstroke was small, it was complementary to the difference in concomitant translatory forces, and therefore the total force was substantially lower during Mode 1 than during Mode 2 (Fig. 19G). We found no significant differences in force inclination between modes (data not shown).

Finally, we compared the influence of mode on mean

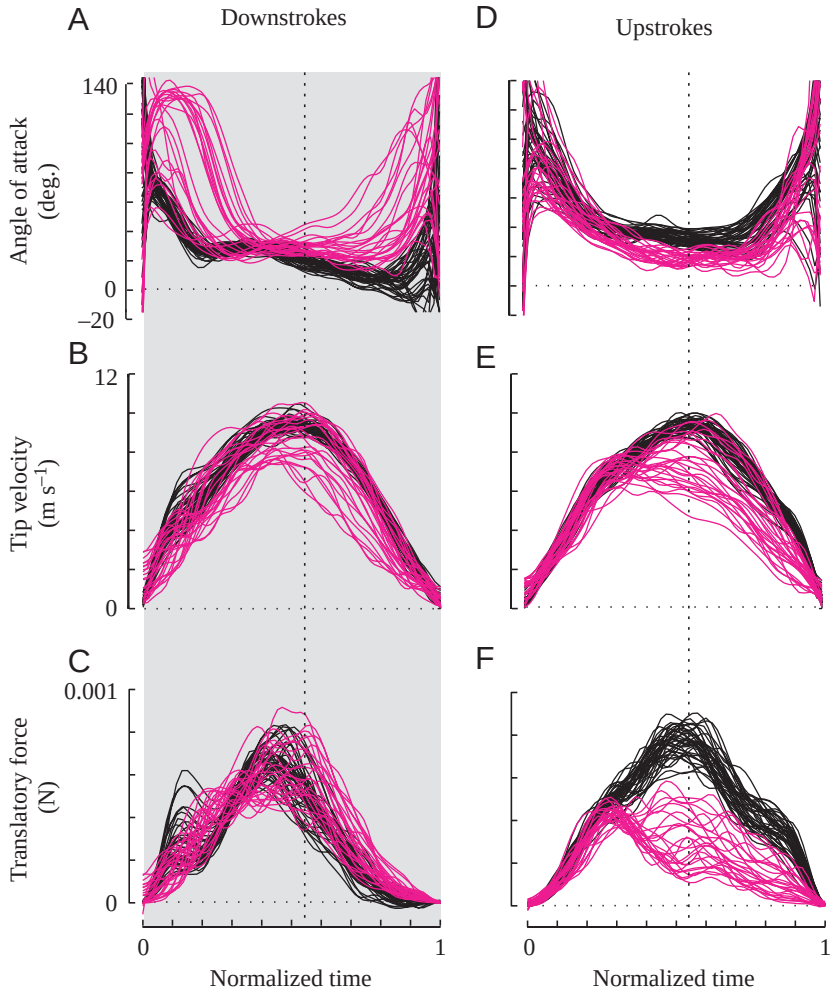

Fig. 17. Comparison of temporal variation in angle of attack, tip velocity and translatory force between modes. Time course of each parameter over the downstroke and upstroke shown along a normalized time axis. Mode 2 strokes are shown in black, and Mode 1 strokes are shown in pink. Mid-stroke was defined as a normalized time of 0.55, indicated by the vertical dotted lines. (A) Angles of attack over the downstroke. (B) Tip velocities over the downstroke. (C) Translatory forces over the downstroke. (D) Angles of attack over the upstroke. (E) Tip velocities over the upstroke. (F) Translatory forces over the upstroke.

resultant forces and moments. Due to the delay in dorsal rotation, the total mean force was slightly lower within Mode 1 downstrokes than within Mode 2 downstrokes (Fig. 20B). By comparison, due to the decrease in both translatory and rotational forces during the upstroke, the total mean force was substantially lower during Mode 1 upstrokes than within Mode 2 upstrokes (Fig. 20G). The relatively small difference in force magnitudes within the downstroke, as well as an equivalent range of force inclinations (Fig. 20C), resulted in a similar relationship between downstroke deviation and lift (Fig. 20D) and roll (Fig. 20E) for both modes. The relatively large difference in force magnitudes between modes during the upstroke resulted in an overall decrease in thrust (Fig. 20I) and yaw (Fig. 20J) during Mode 1 strokes relative to Mode 2. Although the force inclination during the upstroke varied within Mode 1 as within Mode 2 (Fig. 20H), upstroke lift

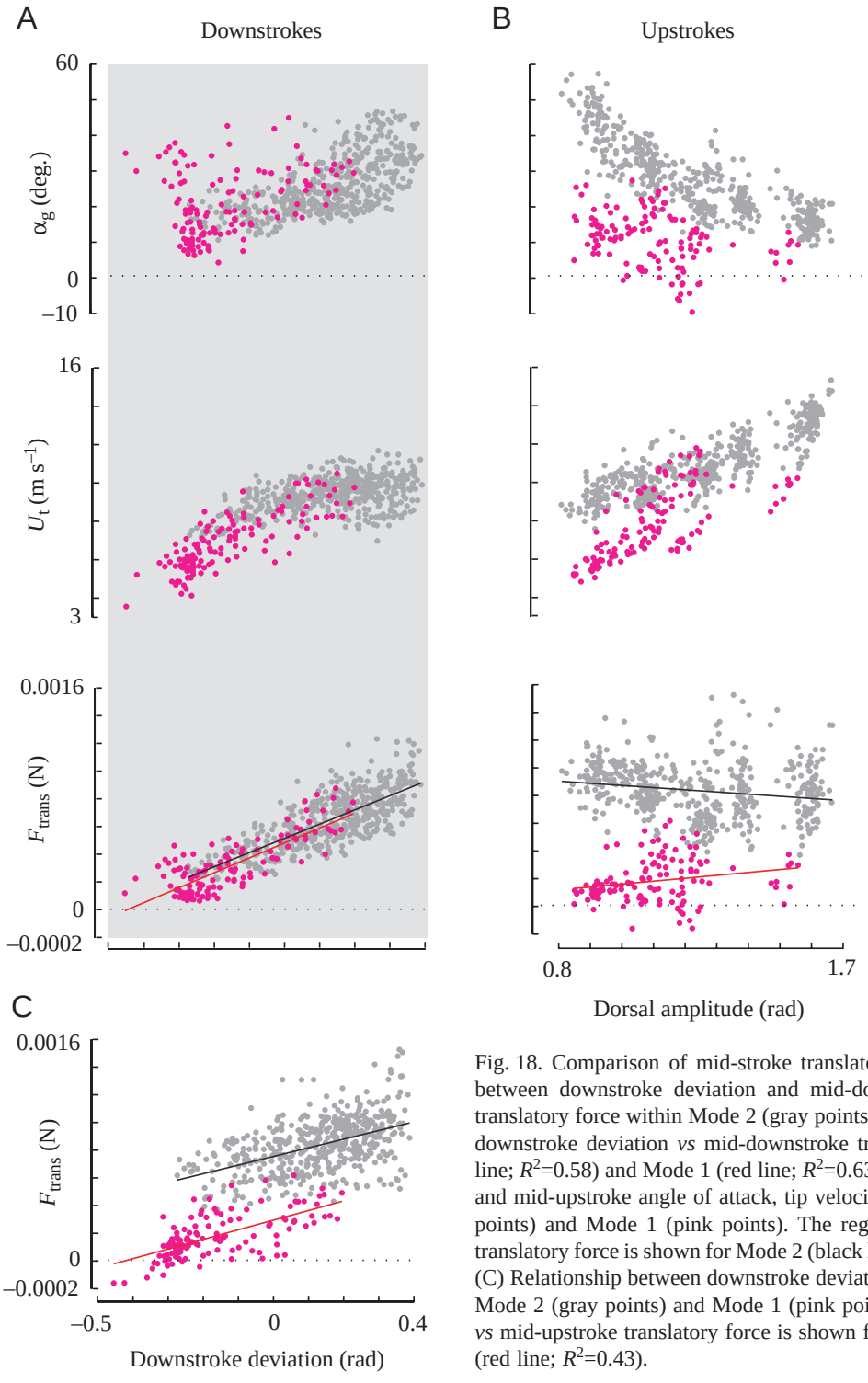

Fig. 18. Comparison of mid-stroke translatory forces between modes. (A) Relationship between downstroke deviation and mid-downstroke angle of attack, tip velocity and translatory force within Mode 2 (gray points) and Mode 1 (pink points). The regression of downstroke deviation *vs* mid-downstroke translatory force is shown for Mode 2 (black line; R^2=0.58) and Mode 1 (red line; R^2=0.63). (B) Relationship between dorsal amplitude and mid-upstroke angle of attack, tip velocity and translatory force within Mode 2 (gray points) and Mode 1 (pink points). The regression of dorsal amplitude *vs* mid-upstroke translatory force is shown for Mode 2 (black line; R^2=0.04) and Mode 1 (red line; R^2=0.05). (C) Relationship between downstroke deviation and mid-upstroke translatory force within Mode 2 (gray points) and Mode 1 (pink points). The regression of downstroke deviation *vs* mid-upstroke translatory force is shown for Mode 2 (black line; R^2=0.23) and Mode 1 (red line; R^2=0.43).

during Mode 1 was small and did not vary considerably [mean upstroke lift, $5.5\times10^{-5}\pm3\times10^{-5}$ N (S.D.)]. Therefore, the upstroke roll was also small during Mode 1 [mean upstroke roll, $2\times10^{-7}\pm1\times10^{-7}$ Nm (S.D.)].

In conclusion, the primary role of a shift in mode was to change the thrust, and, as a consequence, yaw torque generated during the upstroke.

Comparison of calculated forces with measured forces

Although wingbeat frequency is an important kinematic

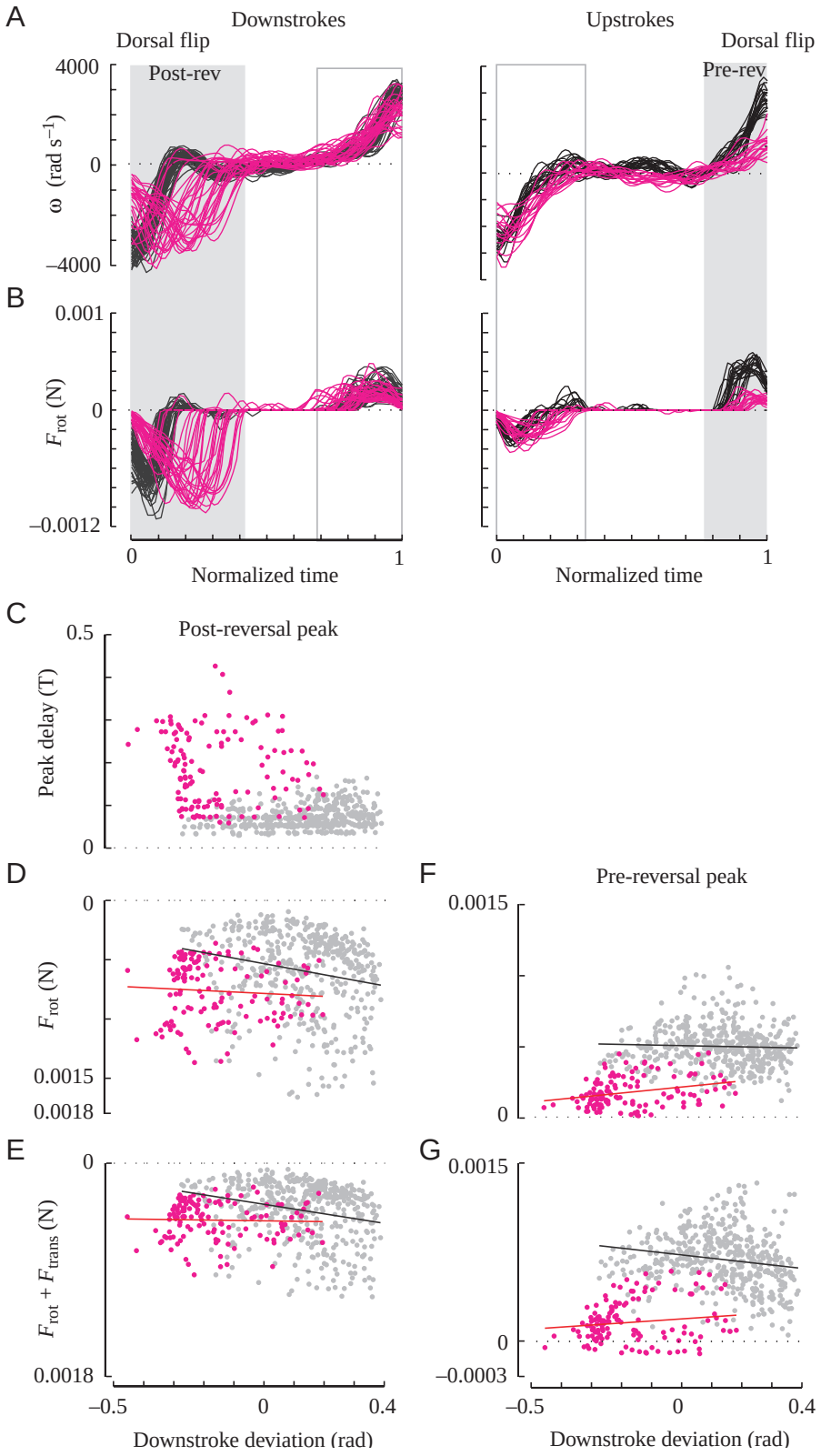

Fig. 19. Comparison of rotational forces between modes. (A) Time course of rotational velocities and (B) time course of rotational forces within Mode 2 (black) and Mode 1 (pink). The filled gray box indicates the dorsal rotation, and the open gray box indicates the ventral rotation. For the dorsal rotation, the pre-reversal portion occurs at the end of the upstroke, and the post-reversal portion occurs at the beginning of the downstroke. (C–G) The following data are for the experimental population. Correlation between downstroke deviation and (C) post-reversal normalized time delay of rotational force peak, (D) post-reversal peak rotational force, (E) post-reversal total force peak, (F) pre-reversal peak rotational force and (G) pre-reversal total force peak for Mode 2 (gray points; black line regression) and Mode 1 (pink points; red line regression).

parameter that affects aerodynamic forces through changes in wingtip velocity, we found it remained relatively constant relative to the other observed changes in wingbeat trajectory (Fig. 4). Within the experimental population, flies fell into roughly two frequency groups. Five individuals flew with a mean wingbeat frequency of 155.2±5.3 Hz (S.D.), and two individuals flew at a mean of 129.4±4.5 Hz (S.D.) (Fig. 21A). Both modes were represented within each frequency group. In order to make comparisons across the population of the effects specific to changes in wingbeat trajectory, in the preceding

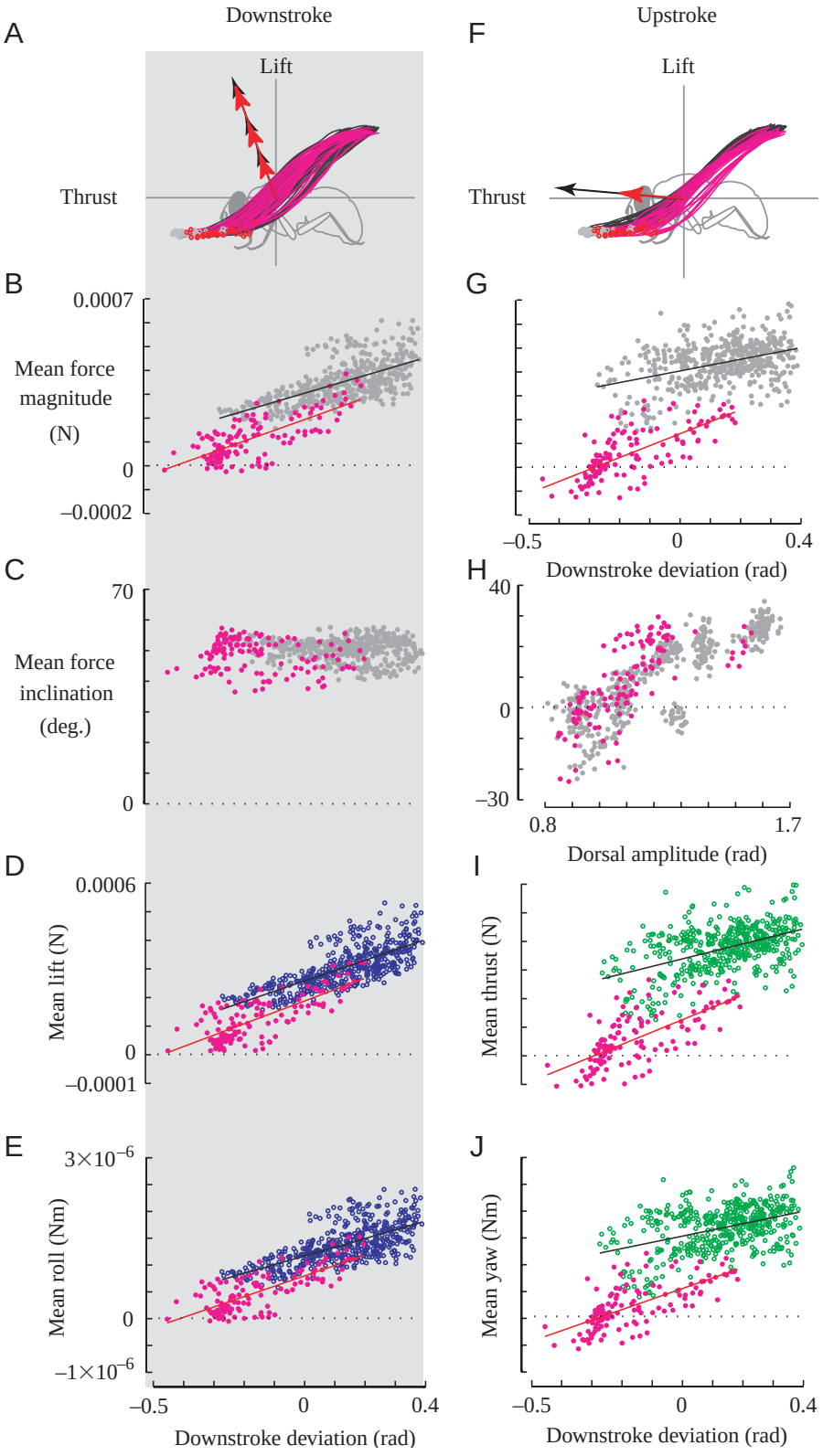

Fig. 20. Mean force vector and resultant directional forces and moments. (A) Schematic illustrating the difference in mean force vector during the downstroke between modes. While force magnitude is similarly modulated within each mode, the mean forces can be slightly lower during Mode 1. Correlation between downstroke deviation and downstroke (B) mean force magnitude and (C) mean force inclination for Mode 2 (gray points; black line regression) and Mode 1 (pink points; red line). Correlation between downstroke deviation and downstroke (D) mean lift and (E) mean roll for Mode 2 (blue points; black line) and Mode 1 (pink points; red line). (F) Schematic illustrating the difference in mean force vector during the upstroke between modes. While force inclination is similarly modulated within each mode (not shown), the mean force magnitudes are much lower during Mode 1. (G) Correlation between downstroke deviation and upstroke mean force magnitude. (H) Correlation between dorsal amplitude and upstroke mean force inclination. Correlation between downstroke deviation and upstroke (I) mean thrust and (J) mean yaw for Mode 2 (green points; black line) and Mode 1 (pink points; red line).

sections we normalized the instantaneous wingtip velocities within each stroke with respect to the cycle period. With this normalization, the relationship between downstroke deviation and the calculated mean force magnitude overlapped for the two frequency populations (Fig. 21B).

However, when we reproduced each fly's kinematics using the dynamically scaled mechanical model, we scaled the wingtip velocities so as to maintain the observed differences in wingbeat frequency. Therefore, we evaluated the difference between our calculated force magnitudes and the forces

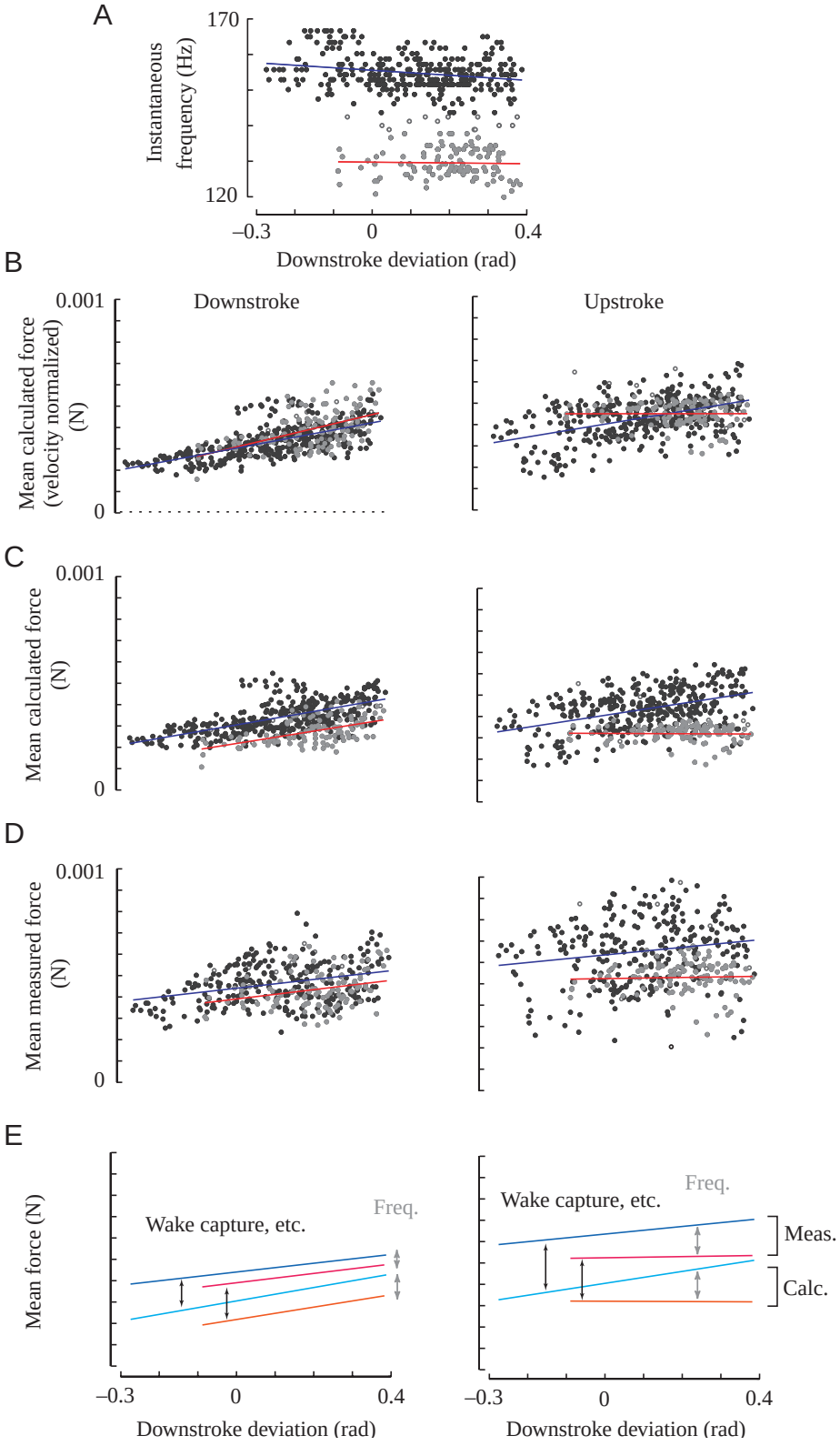

Fig. 21. Mean calculated *vs* measured forces for Mode 2 wingstrokes. (A) Two frequency preferences displayed by the experimental population, mean 155 Hz (black points; blue line) and mean 129 Hz (gray points; red line). (B) Mean calculated force magnitudes for the two frequency groups when wingtip velocity is normalized for a wingbeat period of 0.0065 ms. (C) Mean calculated forces for the two frequency groups when wingtip velocity is not normalized. (D) Mean measured forces for the two frequency groups. (E) Regressions from C and D shown together. The relationship between the calculated forces and downstroke deviation and between the measured forces and downstroke deviation is roughly the same. The difference in forces due to wingbeat frequency is roughly the same for calculated and measured forces. The measured forces are larger than the calculated forces by a roughly constant amount.

measured using the mechanical model by making the comparison separately within the two frequency groups. Fig. 21C illustrates how the relationship between downstroke deviation and the calculated mean force magnitude differs for the two frequency groups when tip velocity is not normalized. The mean difference between the downstroke regressions was $8.8\times10^{-5}\pm6.8\times10^{-6}$ N (S.D.), and the mean difference between the upstroke regressions was $1.3\times10^{-4}\pm2.1\times10^{-5}$ N. The relationship between downstroke deviation and the measured mean force magnitude was very similar, although the scatter among points was larger (Fig. 21D). The mean difference between the downstroke regressions was $4.9\times10^{-5}\pm1.4\times10^{-6}$ N, and the mean difference between the upstroke regressions was $1.4\times10^{-4}\pm1.7\times10^{-5}$ N. Therefore, the effect of the difference in wingbeat frequency on differences in measured force magnitude was very similar to its estimated effect on differences in calculated force magnitude, although the limited range of frequencies did not permit a correlational analysis. The regressions from Fig. 21C and Fig. 21D are shown together in Fig. 21E. For each wingbeat cycle, the measured force was always larger than the calculated force, primarily due to the unexplained force transient at the beginning of each half-stroke as shown in Fig. 3C. However, the relationship between downstroke deviation and force magnitude was roughly the same for calculated and for measured forces.

The difference between calculated and measured forces was roughly the same for both frequency groups (Table 1). The difference was only slightly smaller for Mode 1 strokes than for Mode 2 strokes, given the standard deviations (Table 1). Overall, we found no systematic variation in the magnitude of error between measured and calculated forces, and the random error was small relative to the total mean forces. Therefore, the trends described using the theoretical quasi-steady model were preserved in our measurements using the dynamically scaled mechanical model.

Discussion

By combining detailed measurements of kinematics and muscle activity patterns with an analysis of aerodynamic output, we were able to identify distinct functional consequences of neuromuscular activity. This integrated input–output analysis indicates that concerted, multi-dimensional alterations in the time course of wing motion within each wingbeat cycle are important for a functionally specific manipulation of the aerodynamic force vector. The concerted changes in multiple kinematic parameters are consistent with the complexity of the fly wing hinge, which consists of sclerites that can shift and rotate simultaneously in response to muscle tension (for review, see Dickinson and Tu, 1997). The characteristic firing phase preferences of each steering muscle are most likely important for control of kinematic alterations specific to different parts of the wingbeat cycle. Changes in basalare muscle activity were correlated with changes in downstroke deviation and a set of associated kinematic alterations through the wingbeat cycle that resulted in a strong modulation of the downstroke force and a weak modulation of the upstroke force (Fig. 22A). During activity in the pterale III muscles (Mode 2), the upstroke force remained relatively high (Fig. 22A). Activity in the I1 muscle was correlated with a qualitative shift in wing kinematics (Mode 1), which resulted in a decrease in the force generated during the upstroke relative to Mode 2 (Fig. 22B). Changes in dorsal amplitude were part of a coordinated alteration in wing motion that changed the force inclination during the upstroke without affecting the force magnitude (Fig. 22C). These changes occurred independent of downstroke deviation and mode and did not match activity in any of the recorded steering muscles. Therefore, the basalare muscles primarily controlled lift and roll by varying the downstroke force, the muscles of pteralae III and I controlled thrust and yaw by changing the upstroke force, and an unknown muscle group controlled lift and roll by varying the upstroke force inclination.

Each of the three mechanisms of neuromuscular control – downstroke deviation, mode and dorsal amplitude – involved multiple aerodynamic mechanisms for their effect on the total aerodynamic force vector. Although we organized our analysis according to the three features of wing motion we found to be independently controlled with respect to patterns of muscle activity, these categories also encompassed many of the types of kinematic variation that have been noted previously. Kinematic parameters that have been measured in prior studies of insect flight include stroke amplitude, stroke position or deviation, stroke inclination, degree of pronation/supination, differences in reversal timing, speed and timing of rotation, and wing deformation (e.g. camber and torsion) (for review, see Kammer, 1985; Taylor, 2001). Due to the difficulty of obtaining simultaneous, multi-dimensional, time-resolved images of wing motion, these kinematic parameters have generally been considered as separate categories of modulation. However, our results suggest that these features of the wing stroke are not varied independently and that their coupling has important functional consequences. For instance, changes in downstroke deviation involve concerted modulation of almost all the components listed above. The combined result is a positively correlated change in both the geometrical angle

Table 1. *Difference between mean measured force and mean calculated force*

	Downstroke		Upstroke	
	Mean (N)	S.D. (N)	Mean (N)	S.D. (N)
Mean wingbeat frequency 129 Hz				
Mode 2*	1.7×10^{-4}	4.5×10^{-5}	2.1×10^{-4}	5.1×10^{-5}
Mode 1	1.1×10^{-4}	6.9×10^{-5}	1.1×10^{-4}	8.0×10^{-5}
Total	1.4×10^{-4}	6.3×10^{-5}	1.8×10^{-4}	8.3×10^{-5}
Mean wingbeat frequency 155 Hz				
Mode 2*	1.4×10^{-4}	7.0×10^{-5}	2.2×10^{-4}	10.8×10^{-5}
Mode 1	0.7×10^{-4}	10.1×10^{-5}	1.4×10^{-4}	10.6×10^{-5}
Total	1.3×10^{-4}	8.0×10^{-5}	1.9×10^{-4}	9.8×10^{-5}

*Data shown in Fig. 21.

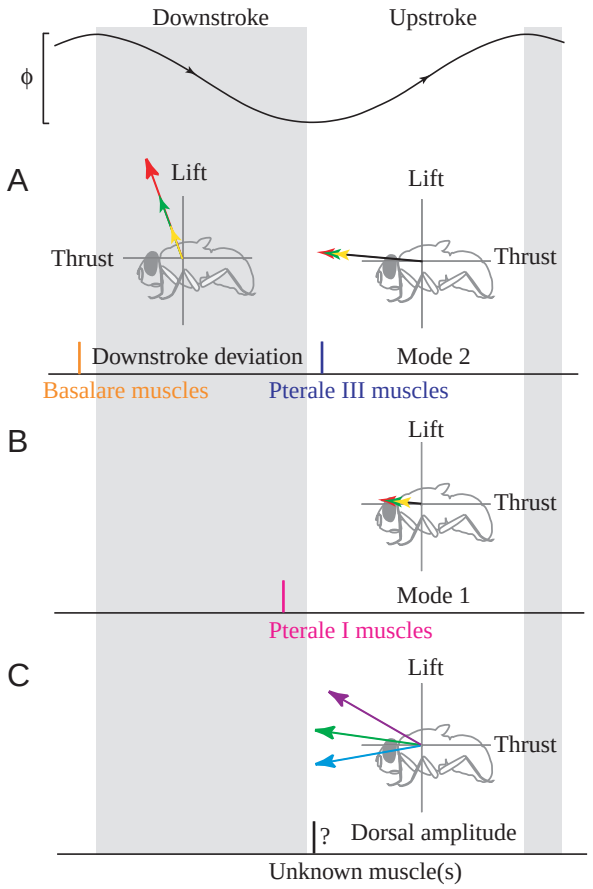

Fig. 22. Summary diagram of the relationship between steering muscle activity and control of the aerodynamic force vector. (A) Firing phase preference of the basalare muscles (left). Basalare muscle activity is correlated with strong modulation of the downstroke force and weak modulation of the upstroke force magnitude. Firing phase preference of pterale III muscles (right). Upstroke force magnitudes are relatively large during Mode 2. (B) Firing phase preference of muscle I1. Upstroke force magnitudes are much smaller during Mode 1 than during Mode 2. (C) Presumed firing phase of unknown muscle and modulation of the upstroke force inclination correlated with dorsal amplitude.

of attack and the tip velocity during the downstroke, which alters the force magnitude without large changes in force inclination. Conversely, the concerted changes associated with dorsal amplitude involve a negative correlation between the angle of attack and the tip velocity during the upstroke, and this allows for changes in force inclination without changes in force magnitude.

Rather than the independent control of each kinematic mechanism of force generation (i.e. angle of attack, tip velocity and rotation), it is the ability to control specific complexes of these parameters during downstrokes and upstrokes independently that allows *Calliphora* to control specific forces and moments. It has long been suggested that flies tend to generate the majority of lift during the downstroke and thrust during the upstroke (Buckholz, 1981; Nachtigall, 1966). However, kinematic mechanisms by which lift and thrust are de-coupled through differences in downstroke and upstroke kinematics have only been hypothesized (Kammer, 1985; Nachtigall and Roth, 1983). We have found that *Calliphora* can indeed control the angle of attack and tip velocity of downstrokes and upstrokes independently. In addition, modulation of ventral rotation complements the modulation of the downstroke translatory force, and modulation of dorsal rotation complements modulation of the upstroke translatory force.

The manipulation of wing kinematics over each stroke involves a system of mechanical linkages that converts the configuration changes imposed by the steering muscles at the wing hinge to the concerted changes in stroke kinematics. The coupling among kinematic parameters may result from these mechanical linkages or from stereotyped patterns of motor neuron activation. Within the group of steering muscles recorded in this study, we noticed a strong tendency for low-frequency basalare muscle activity to be paired with elevated I1 activity and for high-frequency basalare muscle activity to be paired with elevated activity in the muscles of pterale III during steering reactions. The aerodynamic analysis indicates that this gross coupling results in a tendency to actively pair the smallest roll with the smallest yaw torques and the largest roll with the largest yaw torques. This is consistent with the strongest turns measured in free flight being a characteristic banked turn (Schilstra and van Hateren, 1999; Wagner, 1986). Similarly, some of the correlations between kinematic parameters such as angle of attack and tip velocity quantified in this study may be due to consistent patterns of activity in the other unrecorded muscles, rather than to a coupling within the mechanical linkage. Conversely, variation in the temporal firing patterns of the recorded muscles III1 (within Mode 2) and I1 (within Mode 1) may have contributed to some of the unexplained variation within our dataset.

Tests of the context dependence of the concerted changes in wing motion observed in this study will depend on improvements in several inter-related areas of analysis. Additional neuromuscular and kinematic mechanisms of control will most likely be identified through an increase in the number of muscles recorded and a larger range of quantified kinematic variation. We have probably not captured the full range of wing motion within *Calliphora*'s repertoire. For example, although our results suggest that changes in wingbeat frequency are independent of other changes in wing kinematics, we cannot discount the possibility that frequency may be controlled together with other aspects of the wingbeat trajectory but simply were not observed in our study. In addition, another level of complexity involves variations in wing deformation, which we were unable to measure. Although there is no evidence that flies can actively alter wing deformation, especially during rotation when wing torsion is most pronounced (Ennos, 1988), we observed considerable wing deformation through the duration of the upstroke. Such effects might be due to either wing inertia or aeroelastic effects (Combes and Daniel, 2003). Whether or not they are controlled by the fly, unsteady mechanisms such as Nachtigall's swing

mechanism (Nachtigall, 1979, 1981) or Ellington's flex mechanism (Ellington, 1984b) may cause additional modulations of force unaccounted for in this study. A better understanding of the control of forces will also require empirical tests of the factors affecting the wake capture force. Although we found no evidence for controlled variation in the wake capture force, it may vary with respect to some as yet unknown kinematic variable or with varying free-flight conditions.

Most importantly, although we have identified examples of kinematic mechanisms by which different aspects of the aerodynamic force vector can be controlled independently in one wing, the total aerodynamic output will depend on the coordinated control of both wings. The contribution of the total aerodynamic forces and moments to motion of the body will depend on a number of other factors. These include the effects of gravity, inertia, body drag, advance ratio, the effective angle of attack during body translation, and changes in the center of mass due to motion of the legs and abdomen. A more complete description of the influence of wing kinematics on flight behavior will require analysis of the aerodynamic forces within the context of the combined effect of all these factors on the resultant body orientation, flight direction and flight speed. For instance, forward velocity can also contribute to differences in the relative contribution of downstrokes and upstrokes to the flight path (Dudley and Ellington, 1990b; Ellington, 1995; Willmott and Ellington, 1997b). Future experiments incorporating the effect of body translation on the aerodynamics of force generation will be an important step toward a better understanding of flight control.

As our understanding of the variability of wing kinematics and its contributions to insect flight behavior improves, it will be interesting to begin comparisons across species. Although Diptera share a similar flight-related musculo-skeletal architecture, species differ in their ability to hover, fly backwards or sideways. Continued studies of the independent kinematic control parameters of flies may lead to a better understanding of the diversity of flight behaviors and pursuit strategies among flying insects.

List of symbols

$\bar{c}$	mean chord length
$\hat{c}(\hat{r})$	non-dimensional chord length
C_{Dt}	translational drag coefficient
C_{Lt}	translational lift coefficient
C_{rot}	experimental rotational force coefficient
$\mathbf{F_N}$	three-dimensional aerodynamic force vector normal to the wing surface
F_{N}	total aerodynamic force normal to the wing surface
F_{rot}	rotational force normal to the wing surface
F_{trans}	translational force normal to the wing surface
M	Moment about estimated center of mass of the aerodynamic force vector
$\hat{r}$	non-dimensional radial position along wing length
r	position vector of wing's center of area
R	wing length
$\hat{r}_2^2(S)$	non-dimensional second moment of area
S	surface area of wing
t	time
U_{t}	wingtip velocity
α	morphological wing angle
α_{g}	geometric angle of attack
ϕ	wing elevation angle
ν	kinematic viscosity
θ	wing deviation angle
θ_{F}	force inclination relative to longitudinal body axis
ρ	density of fluid
ω	rotational angular velocity($=\dot{\alpha}$)
$\hat{\omega}$	non-dimensional angular velocity

We would like to thank S. P. Sane and W. B. Dickson for their invaluable assistance with the aerodynamics calculations and programming of the mechanical model. The manuscript was greatly improved by critical comments from S. L. Lehman and two anonymous referees. This work was supported by grants from the Packard Foundation and the National Science Foundation (IBN-0217229).

References

Balint, C. N. and Dickinson, M. H. (2001). The correlation between wing kinematics and steering muscle activity in the blowfly *Calliphora vicina*. *J. Exp. Biol.* **204**, 4213-4226.

Blondeau, J. (1981). Aerodynamic capabilities of flies, as revealed by a new technique. *J. Exp. Biol.* **92**, 155-163.

Buckholz, R. H. (1981). Measurements of unsteady periodic forces generated by the blowfly flying in a wind tunnel. *J. Exp. Biol.* **90**, 163-173.

Cloupeau, M., Devillers, J. F. and Devezeaux, D. (1979). Direct measurements of instantaneous lift in desert locust; comparison with Jensen's experiments on detached wings. *J. Exp. Biol.* **80**, 1-15.

Combes, S. A. and Daniel, T. L. (2003). Into this air: contributions of aerodynamic and inertial-elastic forces to wing bending in the hawkmoth *Manduca sexta*. *J. Exp. Biol.* **206**, 2999-3006.

Craven, P. and Wahba, G. (1979). Smoothing noisy data with spline functions. *Numerische Mathematik* **31**, 377-403.

Dickinson, M. (1996). Unsteady mechanisms of force generation in aquatic and aerial locomotion. *Am. Zool.* **36**, 537-554.

Dickinson, M., Lehmann, F.-O. and Sane, S. P. (1999). Wing rotation and the aerodynamic basis of insect flight. *Science* **284**, 1954-1960.

Dickinson, M. H. and Tu, M. S. (1997). The function of Dipteran flight muscle. *Comp. Biochem. Physiol. A* **116**, 223-238.

Dudley, R. and Ellington, C. (1990a). Mechanics of forward flight in bumblebees. I. Kinematics and morphology. *J. Exp. Biol.* **148**, 19-52.

Dudley, R. and Ellington, C. (1990b). Mechanics of forward flight in bumblebees. II. Quasi-steady lift and power requirements. *J. Exp. Biol.* **148**, 53-88.

Ellington, C. P. (1984a). The aerodynamics of insect flight. II. Morphological parameters. *Phil. Trans. R. Soc. Lond. B* **305**, 17-40.

Ellington, C. P. (1984b). The aerodynamics of insect flight. IV. Aerodynamic mechanisms. *Phil. Trans. R. Soc. Lond. B* **305**, 79-113.

Ellington, C. P. (1984c). The aerodynamics of insect flight. VI. Lift and power requirements. *Phil. Trans. R. Soc. Lond. B* **305**, 145-181.

Ellington, C. P. (1995). Unsteady aerodynamics of insect flight. In *Biological Fluid Dynamics* (ed. C. P. Ellington and T. J. Pedley), pp. 109-129. Cambridge: The Company of Biologists.

Ennos, A. R. (1988). The inertial cause of wing rotation in Diptera. *J. Exp. Biol.* **140**, 161-169.

Ennos, A. R. (1989). The kinematics and aerodynamics of the free flight of some Diptera. *J. Exp. Biol.* **142**, 49-85.

Faust, R. (1952). Untersuchungen zum Halterenproblem. *Zool. Jb. Allg. Zool. Physiol.* **63**, 325-366.

Fry, S. N., Sayaman, R. and Dickinson, M. H. (2003). The aerodynamics of free-flight maneuvers in *Drosophila*. *Science* **300**, 495-498.

Heide, G. (1968). Flugsteuerung durch nicht-fibrilläre Flugmuskeln bei der Schmeißfliege *Calliphora*. *Z. Vergl. Physiol.* **59**, 456-460.

Hengstenberg, R., Sandeman, D. C. and Hengstenberg, B. (1986). Compensatory head roll in the blowfly *Calliphora* during flight. *Proc. R. Soc. Lond. Ser. B* **227**, 455-482.

Kammer, A. E. (1985). Flying. In *Comprehensive Insect Physiology, Biochemistry and Pharmacology*, vol. 5 (ed. G. A. Kerkut and L. I. Gilbert), pp. 491-552. New York: Pergamon Press.

Kutsch, W., Berger, S. and Kautz, H. (2003). Turning maneuvers in free-flying locusts: two-channel radio-telemetric transmission of muscle activity. *J. Exp. Zool.* **299A**, 139-150.

Lehmann, F.-O. and Dickinson, M. H. (1997). The control of wing kinematics and flight forces in fruit flies (*Drosophila* spp.). *J. Exp. Biol.* **201**, 385-401.

Nachtigall, W. (1966). Die Kinematik der Schlagflügelbewegungen von Dipteren. Methodische und Analytische Grundlagen zur Biophysik des Insektenflugs. *Z. Vergl. Physiol.* **52**, 155-211.

Nachtigall, W. (1979). Rasche richtungsänderungen und torsionen schwingender fliegenflügel und hypothesen über zugeordnete instationäre strömungseffekte. *J. Comp. Physiol. A* **133**, 351-355.

Nachtigall, W. (1981). Insect flight aerodynamics. In *Locomotion and Energetics in Arthropods* (ed. C. F. Herreid and C. R. Fourtner), pp. 127-162. New York: Plenum Press.

Nachtigall, W. and Roth, W. (1983). Correlations between stationary measurable parameters of wing movement and aerodynamic force production in the blowfly (*Calliphora vicina* R.-D.). *J. Comp. Physiol.* **150**, 251-260.

Sane, S. P. and Dickinson, M. H. (2001). The control of flight force by a flapping wing: lift and drag production by a flapping wing. *J. Exp. Biol.* **204**, 2607-2626.

Sane, S. P. and Dickinson, M. H. (2002). The aerodynamic effects of wing rotation and a revised quasi-steady model of flapping flight. *J. Exp. Biol.* **205**, 1087-1096.

Schilstra, C. and van Hateren, J. H. (1999). Blowfly flight and optic flow I. Thorax kinematics and flight dynamics. *J. Exp. Biol.* **202**, 1481-1490.

Spüler, M. and Heide, G. (1978). Simultaneous recordings of torque, thrust and muscle spikes from the fly *Musca domestica* during optomotor responses. *Z. Naturforsch* **33C**, 455-457.

Srinivasan, M. V. (1977). A visually-evoked roll response in the housefly. Open-loop and closed-loop studies. *J. Comp. Physiol. A* **119**, 1-14.

Taylor, G. K. (2001). Mechanics and aerodynamics of insect flight control. *Biol. Rev.* **76**, 449-471.

Thüring, D. A. (1986). Variability of motor output during flight steering in locusts. *J. Comp. Physiol. A* **158**, 653-664.

Vogel, S. (1967). Flight in *Drosophila*. II. Variations in stroke parameters and wing contour. *J. Exp. Biol.* **46**, 383-392.

Wagner, H. (1986). Flight performance and visual control of flight of the free-flying housefly (*Musca domestica* L.). I. Organization of the flight motor. *Phil. Trans. R. Soc. Lond. B* **312**, 527-551.

Waldman, B. and Zarnack, W. (1988). Forewing movements and motor activity during roll maneuvers in flying desert locusts. *Biol. Cybern.* **59**, 325-335.

Weis-Fogh, T. and Jensen, M. (1956). Biology and physics of locust flight. I. Basic principles in insect flight. A critical review. *J. Exp. Biol.* **239**, 415-458.

Wilkin, P. J. and Williams, M. H. (1993). Comparison of the instantaneous aerodynamic forces on a sphingid moth with those predicted by quasi-steady aerodynamic theory. *Physiol. Zool.* **66**, 1015-1044.

Willmott, A. P. and Ellington, C. P. (1997a). The mechanics of flight in the hawkmoth *Manduca sexta*. I. Kinematics of hovering and forward flight. *J. Exp. Biol.* **200**, 2705-2722.

Willmott, A. P. and Ellington, C. P. (1997b). The mechanics of flight in the hawkmoth *Manduca sexta*. II. Aerodynamic consequences of kinematic and morphological variation. *J. Exp. Biol.* **200**, 2723-2745.

Wortmann, M. and Zarnack, W. (1993). Wing movements and lift regulation in the flight of desert locusts. *J. Exp. Biol.* **182**, 57-69.

Zanker, J. M. (1990). The wing beat of *Drosophila melanogaster*. III. Control. *Phil. Trans. R. Soc. Lond. B* **327**, 45-64.

Zanker, J. M. and Gotz, K. G. (1990). The wing beat of *Drosophila melanogaster*. II. Dynamics. *Phil. Trans. R. Soc. Lond. B* **327**, 19-44.

Zarnack, W. (1988). The effect of forewing depressor activity on wing movement during locust flight. *Biol. Cybern.* **59**, 55-70.